HHS Public Access

Author manuscript

J Immunol. Author manuscript; available in PMC 2023 April 01.

Published in final edited form as:

J Immunol. 2022 April 01; 208(7): 1742–1754. doi:10.4049/jimmunol.2100768.

Influence of self-MHC class I recognition on the dynamics of Natural Killer cell responses to cytomegalovirus infection

Marc Potempa[*], **Oscar A. Aguilar**[*,†], **Maria D. R. Gonzalez-Hinojosa**[*,†], **Iliana Tenvooren**[*,†,‡,§,¶], **Diana M. Marquez**[*,†,‡,§,¶], **Matthew H. Spitzer**[*,†,‡,§,¶], **Lewis L. Lanier**[*,†]

[*] Department of Microbiology and Immunology, University of California, San Francisco, San Francisco, CA, United States

[†] The Parker Institute for Cancer Immunotherapy, San Francisco, CA, United States

[‡] Department of Otolaryngology – Head and Neck Surgery, University of California, San Francisco, San Francisco, CA, United States

[§] Helen Diller Family Comprehensive Cancer Center, University of California, San Francisco, San Francisco, CA, United States

[¶] Chan Zuckerberg Biohub, San Francisco, San Francisco, CA, United States

Abstract

While interactions between inhibitory Ly49 receptors and their self-MHC class I ligands in C57BL/6 mice are known to limit Natural Killer (NK) cell proliferation during mouse cytomegalovirus (MCMV) infection, we created a 36-marker mass cytometry (CyTOF) panel to investigate how these inhibitory receptors impact the NK cell response to MCMV in other phenotypically measurable ways. More than two-thirds of licensed NK cells (i.e. those expressing Ly49C, Ly49I, or both) in uninfected mice had already differentiated into NK cells with phenotypes indicative of antigen encounter (KLRG1$^+$ Ly6C$^-$) or memory-like status (KLRG1$^+$ Ly6C$^+$). These pre-existing KLRG1$^+$ Ly6C$^+$ NK cells resembled known antigen-specific memory NK cell populations in being less responsive to IL-18 and IFNα stimulation *in vitro*, and by selecting for NK cell clones with elevated expression of a Ly49 receptor. During MCMV infection, the significant differences between licensed and unlicensed (Ly49C$^-$ Ly49I$^-$) NK cells disappeared within both cytomegalovirus-specific (Ly49H$^+$) and non-specific (Ly49H$^-$) responses. This lack of heterogeneity carried into the memory phase with only a difference in CD16 expression manifesting between licensed and unlicensed MCMV-specific memory NK cell populations. Our results suggest that restricting proliferation is the predominant effect licensing has on the NK cell population during MCMV infection, but the inhibitory Ly49-MHC interactions that take place ahead of infection contribute to their limited expansion by shrinking the pool of licensed NK cells capable of robustly responding to new challenges.

Corresponding Author: Dr. Lewis L. Lanier, Ph.D., lewis.lanier@ucsf.edu, Phone: (415) 514-0829, Fax: (415) 502-8424.

The authors have no conflicts of interest.

Introduction

Natural Killer (NK) cells monitor other cells for signs of infection or tumorigenesis and eliminate them when identified (1). They accomplish this surveillance through two complementary methodologies: positive recognition of stress ligands, viral proteins, antibody-opsonized cells, or other “non-self” molecules by stimulatory and co-stimulatory receptors (2), and by a “missing-self” mechanism in which inhibitory NK cell receptors (NKRs) are no longer engaged due to the downregulation of MHC class I molecules on unhealthy cells (3). Not all NK cells are equally capable of both strategies, however. Many NKRs, such as those of the Ly49 receptor family in mice and killer cell immunoglobulin-like receptor family in humans, are not guaranteed to be on every NK cell, but instead depend upon a semi-stochastic process during development for expression (4–6). That randomness is further complicated by allelic polymorphisms (7), epigenetic factors (8–10), and environmental conditions (11–13). The end result is a pool of cells comprising almost any given combination of activating and inhibitory NKRs with variegated expression levels of those NKRs. That means some proportion of mature NK cells will lack inhibitory receptors capable of recognizing the MHC class I alleles expressed within the same organism. Such “unlicensed” NK cells at steady-state are unprepared to perform missing-self recognition, and are additionally hyporesponsive to activating stimuli *in vitro* due to a lack of ‘education’ through those inhibitory NKR-MHC interactions (14–16).

Nevertheless, if unlicensed cells are exposed to proinflammatory cytokines, they become as responsive to stimulatory ligands as their licensed NK cell counterparts (i.e. the NK cells expressing inhibitory NKRs engaging self-MHC class I ligands) (14, 15, 17). The unlicensed NK cells may even be at an advantage after cytokine stimulation due to the lack of a concurrent and dominant inhibitory signal (17–19). A clear example of when unlicensed cells are at an advantage is during mouse cytomegalovirus (MCMV) infection of C57BL/6 (B6) mice. Proliferation of NK cells expressing Ly49C and/or Ly49I, which are the NKRs responsible for licensing in B6 mice, is dramatically limited in comparison to unlicensed cells, ultimately making licensed cells less protective (17). This restriction results from the recruitment of the phosphatase SHP-1 to the immunological synapse via the immunoreceptor tyrosine-based inhibitory motifs in the cytoplasmic domains of these receptors (20, 21). SHP-1 then dephosphorylates Vav-1 (2, 18), a guanine nucleotide exchange factor and adaptor molecule with a key role in promoting lymphocyte proliferation (22).

The activities of Vav1 in NK cell function are multifaceted (23–25), however, and whether the impact of licensing on the NK cell response under inflammatory conditions extends beyond proliferation has not been investigated. In pursuit of this aim, we constructed a 36-marker mass cytometry immunophenotyping panel for the analysis of Group 1 ILCs and applied it to the model of MCMV infection of B6 mice. As prefaced, these mice express the inhibitory Ly49C and/or Ly49I receptors on a subset of their NK cells, and those cells are then educated through their interactions with the MHC class I H2-K^b allele (26). B6 mice also express the activating NKR Ly49H, a receptor that enables the direct identification and killing of MCMV-infected cells via recognition of the viral glycoprotein m157 (27, 28). Thus, four critical populations are present within B6 mice: licensed and unlicensed versions

of both m157 antigen-specific and antigen non-specific NK cells. The antigen-specific response additionally results in the formation of an NK cell memory population (29), ultimately allowing us to phenotypically compare licensed and unlicensed cells not only during the expansion and contraction phases, but also in the memory phase of an immune response.

Materials and Methods

Animals.

B6 mice were purchased from the National Cancer Institute at 6 weeks of age and housed in the specific pathogen-free animal facility at the University of California San Francisco (UCSF) thereafter, in accordance with the guidelines of the Institutional Animal Care and Use Committee. *Klra8*$^{-/-}$ (Ly49H-deficient) B6 mice were bred and maintained in the same facility. Germ-free B6 mice were bred and maintained within the UCSF Gnotobiotic Core. Experiments used mice of both genders, aged 8–12 weeks.

MCMV infection.

Wild-type B6 mice were infected with 1000 plaque-forming units (PFU) of Smith strain MCMV via intraperitoneal injection. Ly49H-deficient mice received 1 PFU. Peripheral blood mononuclear cells were acquired at 7 days post-infection (DPI) from mice in the 14, 28, and 35 DPI groups and examined by flow cytometry. Infection status of these animals was confirmed via the observation of KLRG1 upregulation on NK cells and CD8^{+} T cells.

Mass Cytometry Antibodies.

All were commercially available except for the anti-NKR-P1B antibody clone 2D12, which was generously provided by Drs. Wayne Yokoyama and Koho Iizuka (30). Of note, the 5E6 antibody used to differentiate licensed and unlicensed NK cells binds to both Ly49C and Ly49I but is limited in its ability to detect Ly49C^{+} Ly49I^{-} cells in B6 mice due to epitope masking via *cis* interactions with MHC-I molecules (31). 2B4 (m2B4, Biolegend #133501, Panel 1: Sm147, Panel 2: Sm147), CD2 (RM2–5, Biolegend #100102, Panel 1: Dy164, Panel 2: Dy164), CD3 (17A2, Biolegend #100202, Panel 1: Gd157, Panel 2: Gd157), CD8 (53–6.7, Biolegend #100702, Panel 1: Gd155, Panel 2: Gd155), CD11a (M17/4, Biolegend #101101, Panel 1: Dy161, Panel 2: n/a), CD11b (M1/70, Biolegend #101202, Panel 1: In113, Panel 2: Ho165), CD16 (AT154–2, Bio-Rad #MCA5998, Panel 1: Nd144, Panel 2: Nd144), CD19 (6D5, Biolegend #115502, Panel 1: Yb173, Panel 2: Yb173), CD26 (H194–112, Biolegend #137802, Panel 1: n/a, Panel 2: Er167), CD27 (LG.3A10, Biolegend #138302, Panel 1: Ce140, Panel 2: Bi209), CD32 (AT130–5, Bio-Rad #MCA6000, Panel 1: Yb171, Panel 2: Eu153), CD45 (30-F11, Biolegend 103102, Panel 1: In115, Panel 2: In113), CD49b (DX5, Invitrogen #14–5971-85, Panel 1: Sm152, Panel 2: Sm152), CD69 (H1.2F3, Biolegend #104502, Panel 1: Sm154, Panel 2: Sm154), CD90 (30-H12, Biolegend #105302, Panel 1: Yb176, Panel 2: Yb176), CD96 (3.3, Biolegend #131704, Panel 1: Nd146, Panel 2: Nd146), CD127 (A7R34, Biolegend #135002, Panel 1: Nd150, Panel 2: Nd150), CD132 (TUGm2, Biolegend #132304, Panel 1: Nd142, Panel 2: Nd142), CD137 (17B5, Biolegend #106114, Panel 1: Er167, Panel 2: Er166), CD200R1 (OX-110, Biolegend #123902, Panel 1: Ho165, Panel 2: n/a), CEACAM-1 (Mab-CC1, Biolegend #134504, Panel

1: Gd156, Panel 2: Gd156), CXCR6 (SA051D1, Biolegend #151102, Panel 1: Er166, Panel 2: n/a), DNAM-1 (TX42.1, Biolegend #133630, Panel 1: Sm149, Panel 2: Sm149, IFNAR (MAR1–5A3, Biolegend #127302, Panel 1: Nd148, Panel 2: Nd148), IL-18Ra (A17071D, Biolegend #157902, Panel 1: Lu175, Panel 2: Lu175, KLRG1 (2F1, Invitrogen #16–5893, Panel 1: Yb172, Panel 2: Yb172), LAG-3 (C9B7W, Biolegend #125202, Panel 1: n/a, Panel 2: Yb171), Ly6C (HK1.4, Biolegend #128002, Panel 1: Eu151, Panel 2: Pr141), Ly49A (YE1/48.10.6, Biolegend #94015 [discontinued], Panel 1: Dy163, Panel 2: n/a), Ly49C/I (5E6, BD Biosciences #553273, Panel 1: Bi209, Panel 2: Er168), Ly49D (4E5, Biolegend #138302, Panel 1: La139, Panel 2: Eu151), Ly49G2 (4D11, BD Biosciences #555314, Panel 1: Yb174, Panel 2: Yb174), Ly49H (3D10, Biolegend #144702, Panel 1: Pr141, Panel 2: Tb159), NK1.1 (PK136, Biolegend #108702, Panel 1: Gd160, Panel 2: Gd160), NKG2ACE (20d5, Invitrogen #16–5896-85, Panel 1: Gd158, Panel 2: Gd158), NKG2D (CX5, Biolegend #130202, Panel 1: Er170, Panel 2: Er170), NKp46 (29A1.4, Biolegend #137602, Panel 1: Tm169, Panel 2: Tm169), NKR-P1B (2D12, Panel 1: Nd143, Panel 2: Nd143), PD-1 (29F.1A12, Biolegend #135202, Panel 1: Tb159, Panel 2: n/a), TIGIT (1G9, Biolegend #142012, Panel 1: n/a, Panel 2: Dy163).

Antibodies were conjugated to their associated metals with MaxPar X8 labeling reagent kits (DVS Sciences) according to manufacturer instructions, diluted with Candor PBS Antibody Stabilization solution (Candor Bioscience) supplemented with 0.02% sodium azide, and filtered through an UltrafreeMC 0.1 μm centrifugation filter (Millipore) before storage at 4° C. Each metal-bound antibody was titrated on splenocytes collected from untreated wild-type B6 mice or B6 mice that received 150 μg of poly(I:C) via intraperitoneal injection 18-hours ahead of collection.

Sample Preparation for Mass Cytometry.

Spleens were mechanically dissociated using the flat end of the plunger from a 1 mL syringe and filtered through a 40 μm strainer. Following red blood cell lysis using ACK lysis buffer, cells were washed and re-suspended in PBS + 5 mM EDTA (PBS/EDTA). The suspension was then mixed 1:1 with PBS/EDTA containing 100 mM cisplatin (Enzo Life Sciences) for viability staining. After one minute, PBS + 5 mM EDTA + 0.5% bovine serum albumin (CyTOF Staining Media) was added at 1:1. Cells were washed, resuspended in CyTOF Staining Media, and counted.

One million splenocytes from each mouse were transferred into individual staining tubes and stained with metal-conjugated antibodies against CD16 and CD32b for 15 minutes at room temperature in 100 μL volume. Following this initial incubation, an Fc blocking antibody (clone 2.4G2) was mixed into each stain and left for another 15 minutes at room temperature. Cells were washed twice before being stained with a master mix of all remaining metal-conjugated antibodies for 30 minutes at room temperature in 100 μL volume.

For cells stained with the initial panel, following the antibody stain, cells were washed and then fixed for 10 minutes at room temperature using 1.6% paraformaldehyde (PFA) in PBS/EDTA. After another wash with PBS/EDTA, they were resuspended in PBS/EDTA + 10% dimethyl sulfoxide and stored at −80° C for barcoding at a later date. Cells stained

with the updated panel were not frozen, but instead were fixed and kept in 3.2% PFA in PBS/EDTA at 4°C for 3–5 days before proceeding to barcoding.

For barcoding, each sample was thawed, if necessary, washed once, and then resuspended in 1x Barcode Perm Buffer (Fluidigm). Splenocytes from each mouse were labeled with one of 20 distinct combinations of Pd isotopes, as described previously (32). When more than 20 mice were barcoded at once, as during the side-by-side infection of wild-type and Ly49H-deficient mice, samples from each genotype were split evenly between different sets of the barcode combinations. After washing in PBS/EDTA, all cells from each set of 20 barcodes were pooled. Pooled cells were then fixed in a 3.2% PFA in PBS/EDTA solution containing a 1:1000 dilution of a 191/193 Ir DNA intercalator (Fluidigm) and kept at 4° C overnight.

Mass Cytometry Data Acquisition and Normalization.

Just prior to analysis, the barcoded samples were pelleted, washed in CyTOF Staining Media, washed twice more in double-deionized (dd) water, and then resuspended in dd water containing a 1:20 dilution of EQ™ Four Element Calibration Beads (Fluidigm) at a concentration of approximately 10^6 cells/mL. The mixture was filtered through a 35 μm cell strainer and then analyzed on a CyTOF2-Helios mass cytometer (Fluidigm). The resulting data files were normalized using the mass cytometry data normalization algorithm (33), which uses the calibration beads to correct for inconsistencies in sample detection over time.

viSNE/FlowSOM Plot Generation.

After normalization and de-barcoding, live singlets were identified on the basis of DNA and a negative cisplatin stain. Group 1 ILCs were selected initially selected as $CD2^+$ $CD3^-$ $CD19^-$ $2B4^+$ $NK1.1^+$ before revising the phenotype to $CD2^+$ $CD3^-$ $CD8^-$ $CD19^-$ $2B4^+$ CEACAM-$1^{lo/-}$ when splenocytes from infected mice were included in the analysis. Example gating strategies can be found within Supplementary Figure 1. FCS files containing the events isolated as Group 1 ILCs were uploaded into the web-based CytoBank platform (34), and viSNE plots were generated there (35). All files were sampled equally, and all antibody-targeted markers were used for clustering unless otherwise noted. Where applicable, secondary analysis of the viSNE plots was done by FlowSOM (36). FlowSOM clustering was based solely on the tSNE1 and tSNE2 channels, and the hierarchical consensus clustering methodology was employed. The number of metaclusters and clusters were determined based on iterative testing.

HeatMaps Generation.

For heatmaps representing FlowSOM metaclustering results, cluster median and abundances were downloaded from the CytoBank platform. Cluster medians were scaled within each channel as percentage of max and then grouped by metacluster. Values for each channel within a metacluster were then determined as the weighted average of the scaled cluster medians with weighting determined by cluster abundances. Heatmaps were then generated in R (R Core Team, 2020) using the ComplexHeatmap package. The heatmap in Figure 6 was generated by manually gating the four Ly49I and Ly49H subsets with FlowJo software (Tree Star), exporting the event data for each group at each timepoint, and then proceeding

to scale and average the data. To avoid the impact of outliers while scaling the data, the values used for scaling were the medians of the top 100 events within each channel. After generating the heatmap in R, the columns were manually reorganized by time point and Ly49I and Ly49H subsets.

Principal Component Analysis and Euclidean Distance Calculations.

Principal component analysis was performed on data matrices using the basic Stats package in R. For the analysis in Figure 1, the relevant matrix was that which was used to generate the heatmap. For the infection data, Ly49I-positive and -negative subsets were manually gated in FlowJo with the additional separation into Ly49H-positive and -negative subsets if possible. That data was exported, scaled within each channel as percent of max, and then averaged as for the Figure 6 heatmap. In each case, only two components explained more than 10% of the variance. For the calculation of similarity between $Ly49I^+$ and $Ly49I^-$ subsets, the Euclidean distance between all pairs of $Ly49I^+$ and $Ly49I^-$ cells, stratified by Ly49H, at each time point was determined.

Flow Cytometry.

Splenocytes from wild-type or infected mice were isolated by mechanical dissociation through a 0.4 μm cell strainer and freed from red blood cells by treatment with ACK lysis buffer. Surface staining was performed using pre-conjugated antibodies and samples were run on an LSR II cytometer (BD Biosciences). The antibodies used for flow cytometry were: CD2 (RM2–5, BioLegend #100104), CD3ε (145–2C11, BioLegend #100349 and #100330), CD8α (53–6.7, BD Biosciences #612759), CD16 (S17014E, BioLegend #158004), CD19 (6D5, BioLegend #115534 and #115546), CD49b (DX5, BD Biosciences #563063 and #108922), CD90.2 (30-H12, BioLegend #105320), NK1.1 (PK136, BD Biosciences #564144 and BioLegend #108739), 2B4 (m2B4 [B6]458.1 BioLegend, #133516), KLRG1 (2F1, BioLegend #138429), Ly6C (HK1.4, BioLegend #128049), Ly49C (4LO3311, a generous gift from Dr. Wayne Yokoyama (14)), Ly49H (3D10, BioLegend #144710 and BD Biosciences #744260), Ly49I (YLI-90, ThermoFisher #11–5895-82), FcεRIγ (polyclonal, EMD Millipore, # FCABS400F), rabbit IgG isotype control (Polyclonal, Invitrogen, #11–4614-80). An unconjugated anti-CD16/CD32 antibody (clone 2.4G2, UCSF Antibody Core) was used to block non-specific binding. In experiments measuring CD16 expression, cells were stained with the fluorophore-conjugated anti-CD16 antibody prior to treatment with 2.4G2, as the latter blocks binding of the CD16-specific antibody. An example gating strategy is presented in Supplementary Figure 1. Data were analyzed in FlowJo.

In Vitro Stimulation Assays.

Splenocytes were harvested and processed into single cell suspensions and RBC lysed. Cells were then stained for surface markers (NK1.1, NKp46, CD3ε, CD19, Ly6C, KLRG1, Ly49I, and Ly49H) and viability (Zombie Red, BioLegend), and then rested for 1 hour at 37° C in 75 μL of RPMI-1640 (RPMI) supplemented with 2 mM glutamine, 100 U/ml penicillin, 100 μg/ml streptomycin, 50 μg/ml gentamicin, 110 μg/ml sodium pyruvate, 50 μM 2-mercaptoethanol, 10 mM HEPES, and 10% FCS. Splenocytes were then stimulated with IFN-α1 (BioLegend) or IL-18 (BioLegend) in 2-fold dilution series in 75μL of supplemented RPMI, starting at 50 ng/mL or 10 ng/mL, respectively. Cells

were incubated at 37° C for 15 minutes, and then fixed using 150 μL of FluoroFix (BioLegend), followed by permeabilizing using True-Phos Perm buffer as recommended by manufacturer (BioLegend). Cells were then intracellularly stained with antibodies against phospho-STAT1^{Ser727} (S727) (clone A15158B, BioLegend), and phospho-p38 (clone 36/p48 (pT180/pY182), BD Biosciences. Cells were then analyzed using a flow cytometer.

Determination of MCMV Titer.

An aliquot of MCMV at a starting concentration of 10,000 PFU/mL was diluted to 500 PFU/mL using sterile PBS, and then serially diluted by 5-fold to concentration of 100 PFU/mL and 20 PFU/mL. A portion of the 20 PFU/mL aliquot was additionally diluted 2-fold to generate a 10 PFU/mL. Wild-type mice were infected with 100 μL of the original 10,000 PFU/mL aliquot (i.e. 1000 PFU), while Ly49H-deficient mice were infected with 100 μL of each of the four dilutions (50 PFU, 10 PFU, 2 PFU, and 1 PFU). At 7 DPI, the mice were euthanized, and spleens recovered. Spleens were weighed before being mechanically dissociated through a 40 μm cell strainer and suspended in DMEM. DNA was isolated from a portion of the splenocyte suspension using the Reliaprep Blood gDNA miniprep kit (Promega) according to manufacturer's instructions. Real-time PCR was performed with the SYBR Green Master Mix reagent (Invitrogen) under standard conditions. Primers were designed to detect the IE1 gene of MCMV. Forward Primer: 5' – AGCCACCAACATTGACCACGCAC – 3'; Reverse Primer: 5' – GCCCCAACCAGGACACACAACTC – 3'. Copies per reaction were determined and used to calculate the estimated number of copies of IE1 DNA per mg of spleen (37).

Statistical Analysis.

Statistical analyses were made using Prism v9 (GraphPad Software Inc.). Most comparisons were evaluated by two-way ANOVA with the Benjamini and Yekutieli correction, matching cellular subsets isolated from the same mice when possible. Results with $p < 0.05$ were considered significant. Error bars represent standard deviation from the mean unless otherwise noted.

Results

Group 1 ILCs form six major subsets

We devised a 36-marker mass cytometry panel tailored toward Group 1 ILCs (Panel 1), which includes NK cells and ILC1, and first examined splenocytes from uninfected 8-week-old B6 mice. A total of 29,800 Group 1 ILCs (CD2$^+$ CD3$^-$ CD19$^-$ 2B4$^+$ NK1.1$^+$ CEACAM-1$^{lo/-}$) were clustered by viSNE (35) and analyzed by FlowSOM (36) to identify different metaclusters within the data (Figure 1a). Repeated testing showed isolation of ILC1s as a distinct subset required a minimum of 13 metaclusters. These ILC1s were CD49b$^{+/-}$ CD11b$^-$ CD27$^+$ and expressed higher levels of CD69, CD127, and CD200R1 (Figure 1b), as previously reported (38–40). We additionally found ILC1s to express significantly more CD96, CD132, DNAM-1, NKp46, and NKR-P1B compared to all NK cell subsets, and more IL18Ra and NKG2D than all but one NK cell subset (Supplementary Figure 2). The remaining 12 metaclusters were all CD49b$^+$ CD127$^{lo/-}$ CD200R1$^-$ NK cells. However, five pairs of clusters (M2a/b, M3b/c, M4a/b, and M5a/b) differed according to

the same dichotomy – preferential expression of activating Ly49 receptors or NKG2ACE (Figure 1b). Similarly, cells bound or unbound by the antibody clone 5E6, an antibody capable of recognizing both Ly49C and Ly49I (though limited to Ly49I recognition in B6 mice (31)), drove two other bifurcation events (M3a/bc, M4ab/c). These repetitive events suggested an over-partitioning of NK cell subsets, albeit one necessary to draw out the ILC1 population. Omitting these distinctions simplified the 12 NK cell clusters into five.

These five subsets could then be efficiently separated using CD90 and two other markers associated with different stages of NK cell differentiation, KLRG1 and Ly6C (29, 41). Two types of naïve KLRG1^{-} Ly6C^{-} NK cells were present, with the most prominent difference being high or low expression of CD90. The CD90^{hi} clusters stained strongly for CD27, while the trio of CD90^{lo} clusters had middling expression of both CD27 and CD11b (Figure 1c). This identified the CD90^{hi} subset as an immature subset and the CD90^{lo} as an ‘intermediate’ or ‘transitioning’ subset that had not fully matured into CD11b^{+} CD27$^{lo/-}$ cells (42). KLRG1 is upregulated on antigen-experienced, fully mature CD11b^{hi} CD27$^{lo/-}$ NK cells (41), and the two KLRG1^{+} groups identified were split according to the expression or absence of Ly6C. Notably, the KLRG1^{+} Ly6C^{+} phenotype is closely associated with the long-lived memory NK (mNK) cell population present after MCMV infection (29). Combined, these four groups provide a putative sequence of phenotypes depicting NK cell differentiation from an immature subset to a memory state: KLRG1^{-} Ly6C^{-} CD90^{hi} → KLRG1^{-} Ly6C^{-} CD90^{lo} → KLRG1^{+} Ly6C^{-} → KLRG1^{+} Ly6C^{+}.

The fifth NK subset had a phenotype of KLRG1^{-} Ly6C^{+}, which has not been previously characterized. Most features of the KLRG1^{-} Ly6C^{+} subset (e.g. NKp46^{lo}, IFNAR^{lo}, CD2^{lo}) were shared with at least one other subset, but there was no consistency in which subset that was (Supplementary Figure 2). Based on CD11b and CD27 expression, these cells split between intermediate and fully mature subsets (Figure 1c). However, principal component analysis (PCA) paired them most closely with the fully mature KLRG1^{+} Ly6C^{-} subset (Figure 1d). Thus, KLRG1^{-} Ly6C^{+} cells represent a third fully mature NK cell subset. It remains unclear where the KLRG1^{-} Ly6C^{+} subset might reside in the NK cell differentiation pathway or if it follows an entirely alternative pathway. In summary, clustering analysis identified six major group 1 ILC subsets: ILC1s, immature CD90^{hi} KLRG1^{-} Ly6C^{-} NK cells, transitionary CD90^{lo} KLRG1^{-} Ly6C^{-} NK cells, antigen-experienced KLRG1^{+} Ly6C^{-} NK cells, a pre-existing population with a memory-like KLRG1^{+} Ly6C^{+} phenotype, and a novel KLRG1^{-} Ly6C^{+} subset.

Most Ly49I^{+}NK cells in uninfected mice have differentiated into less responsive states

Approximately 75% of the NK cells with a “memory-associated” KLRG1^{+} Ly6C^{+} phenotype in uninfected mice were 5E6-positive (hereafter Ly49I^{+}), accounting for just over one-third of all Ly49I^{+} cells (Figure 2a). If these cells represented a pool of pre-existing memory-like NK cells were established against unknown antigens, then the dominance of unlicensed NK cells during MCMV infection could, in part, be due to the diminished ability of memory and memory-like NK cells to respond to cytokines and heterologous stimuli (43, 44). Consistent with this possibility, these pre-existing KLRG1^{+} Ly6C^{+} cells were CD132^{lo}, IFNAR^{lo}, and IL18Ra^{lo} relative to both immature NK cell subsets (Figure 2b).

We, therefore, measured phosphorylation of p38-MAPK and STAT1 (S727) following *in vitro* stimulation of B6 splenocytes with PMA + ionomycin, IL-18, and IFNα. Reduced levels of phosphorylation were evident in KLRG1$^+$ Ly6C$^+$ cells relative to the other subsets after PMA + ionomycin treatment, as well as after IL-18 and IFNα exposure. Interestingly, stimulation with IL-18 resulted in STAT1 phosphorylation (Figure 2c) despite STAT1 not being a known downstream effector of the IL-18R signaling pathway (45). STAT3, however, is phosphorylated via the MAPK cascade initiated by IL-18 signaling (46), so further crosstalk with STAT pathways is not farfetched. Regardless, the reduced responsiveness of the KLRG1$^+$ Ly6C$^+$ subset to chemical and cytokine stimulation was consistent with characterization of the cells as a pre-existing memory-like NK (pemNK) cell population. Thus, the unlicensed NK cell response dominates during infection not just because Ly49I inhibits proliferation (17), but also because most Ly49I$^+$ cells have pre-differentiated into less responsive antigen-experienced or memory-like states.

Development of pre-existing memory-like NK cells is not dependent upon the commensal microbiota

Despite being an inhibitory receptor, Ly49I's over-representation in the pemNK cells (Figure 2a) suggested it may be key to the formation of this subset, and lending credence to this hypothesis is Ly49I's reported role in NK cell memory development to haptens (47). Upon investigation, Ly49I's median signal intensity (MSI) of staining resembled that of Ly49H on MCMV-specific mNK cells in being significantly elevated on Ly49I$^+$ KLRG1$^+$ Ly6C$^+$ cells (Figure 3a). No other receptor was immediately apparent as a driver of differentiation into KLRG1$^+$ Ly6C$^+$ cells based on this criterion (Supplementary Figure 3), including NKG2A, which has been reported as a licensing molecule (15). We also considered whether the Ly49I$^-$ KLRG1$^+$ Ly6C$^+$ population may be Ly49C$^+$ but appear to be unlicensed due to epitope masking resulting from a strong *cis*-interaction between Ly49C and the MHC-I alleles expressed in B6 mice (31, 48, 49). Upon studies comparing NK cell phenotypes as measured with the 5E6 antibody, the Ly49C-specific 4LO3311 antibody (a generous gift of Dr. Wayne Yokoyama), and the commercially available Ly49I-specific YL1–90 antibody, we found 15–30% of licensed NK cells went undetected by the 5E6 antibody due to epitope masking. However, approximately 20% of KLRG1$^+$ Ly6C$^+$ cells remained absent of both Ly49C and Ly49I expression when stained with the 4LO3311 and TL1–90 antibodies (Figure 3b), closely approximating the contribution of 5E6$^-$ cells to the subset as earlier determined (Figure 2a). Intriguingly, staining using the 4LO3311 and YL1–90 antibodies revealed that only Ly49I exhibited an increased expression density on KLRG1$^+$ Ly6C$^+$ cells (Figure 3c). Ly49C, like NKG2A (Supplementary Figure 3), was expressed to a lesser extent on pemNK cells than naïve NK cells (Figure 3c).

We briefly sought the potential immunogen for Ly49I$^+$ pemNK cells in naïve mice, hypothesizing that the commensal microbiota might be involved due to its effect in boosting the frequency of KLRG1$^+$ NK cells (50) and a suggested relationship to "trained" innate immune memory (51). However, when we analyzed germ-free mice alongside conventionally housed B6 mice, the germ-free mice also possessed these KLRG1$^+$ Ly6C$^+$ NK cells (Figure 3d); there was actually a small, but significant, increase in their frequency compared to conventionally housed mice. Moreover, Ly49I was found on germ-free pemNK

cells at the same frequency as pemNK cells from conventionally housed mice, further diminishing the likelihood that interactions with microbial byproducts produce this subset in B6 mice and suggesting microbiota does not affect licensing (Figure 3e). The MSI of Ly49I was lower on germ-free pemNK, but it was nevertheless still elevated relative to naïve NK cells (Figure 3d). Other differences between naïve and these KLRG1^{+} Ly6C^{+} cells in CD2, IFNAR, IL18Ra, NK1.1, and other markers were all still present in germ-free mice as well (Figure 3f). These data were therefore inconsistent with a driving role for the commensal microbiota in pemNK development.

NKR expression levels vary between licensed and unlicensed cells at steady-state

While the relative lack of KLRG1^{-} Ly6C^{-} Ly49I^{+} NK cells provides an additional explanation for the preferential expansion of unlicensed cells during MCMV infection, we also addressed whether pre-existing differences in phenotype within subsets might contribute. For that, we examined the CD90^{lo} KLRG1^{-} Ly6C^{-} and KLRG1^{+} Ly6C^{-} clusters, each of which separated into two groups based on Ly49I status (Figure 1b). Within each of these cluster pairs, Ly49A, Ly49D, Ly49G2, and NKR-P1B all appeared more frequently on Ly49I^{-} NK cells (Figure 4a) and at higher MSI when present (Figure 4b). There was an important exception to this pattern among the Ly49 receptors, Ly49H. There was no preferential distribution among Ly49I-positive or -negative cells, but Ly49H was expressed at a higher density on Ly49I^{+} cells. NKp46 and NKG2D were similar to Ly49H in that manner, also being expressed more robustly on licensed NK cells. Given the more limited expression of NKR-P1B, an inhibitory receptor engaged by the MCMV immunoevasin m12 (52), and an increased expression of the activating NKRs Ly49H, NKG2D, and NKp46, these data would argue for an *increased* potential of licensed Ly49I^{+} NK cells to respond during MCMV infection. These data, therefore, suggest pre-existing phenotypic differences between licensed and unlicensed cells, when accounting for cellular maturity, do not significantly explain the disparate NK cell responses to MCMV.

A subset of Ly49H^{+} NK cells lose expression of CD16 and NK1.1 during the NK cell expansion phase

Following the characterization of licensed and unlicensed cells at steady-state, we investigated changes in these cells during MCMV infection. Groups of B6 mice received 1000 PFU of salivary gland-derived MCMV and splenocytes from 4-, 7-, 14-, and 35-DPI were analyzed alongside uninfected controls. Immediately apparent was the significant downregulation of two key Group 1 ILC lineage markers: NK1.1 and NKp46 (Figure 5a). This necessitated a revision of the Group 1 ILC phenotype to identify responding NK cells as CD2^{+} CD3^{-} CD8^{-} CD19^{-} 2B4^{+} CEACAM-1$^{lo/-}$ to avoid excluding NK cells in the analysis. A resulting total of 72,785 cells (14,557 per time point) were analyzed by viSNE. Examination of the plots revealed that a few contaminating myeloid and NKT cells were present (Figure 5b), though they combined for no more than 2.5% of the cells at any time point. Thus, the alternative gating strategy was highly effective at isolating Group 1 ILCs without using the traditional NK cell lineage markers for identification of responding NK cells.

Both the Ly49I$^+$ and Ly49I$^-$ NK cells underwent considerable phenotypic change during infection before returning to a near pre-infection state, with the key difference being the expected increase in mNK cells (Figure 5c,d). The non-standard gating strategy additionally revealed the presence of a small group of CD49b$^+$ Ly49H$^+$ NK1.1$^-$ CD16$^-$ NK cells at 4 days DPI (Figure 5e). Though more easily seen in the Ly49I$^-$ subset, these cells were present in both groups. Because NK1.1 and CD16 depend upon FcεRIγ for surface expression, and a subset of NK cells in humans is known to downregulate FcεRIγ following HCMV infection (53, 54), we examined whether these might be a corresponding population in mice. Though we confirmed that 8–10% of CD2$^+$ CD3$^-$ CD8$^-$ CD19$^-$ CEACAM-1$^-$ 2B4$^+$ CD49b$^+$ Ly49H$^+$ cells were NK1.1$^-$ CD16$^-$ at 4 DPI (Figure 5f), such lymphocytes nevertheless retained expression of FcεRIγ at levels equivalent to NK1.1$^+$ CD16$^+$ cells (Figure 5g). The loss of NK1.1 and CD16 expression on these cells was therefore not due to silencing of the FcεRIγ signaling adapter, which occurs in human NK cells responding to CMV.

Licensed and unlicensed cells phenotypically converge during MCMV infection

For the detailed comparison of changes to licensed and unlicensed NK cell phenotypes during primary MCMV infection, NK cells were divided into four populations on the basis of Ly49I and Ly49H expression. While there were observable differences in Ly49H$^+$ and Ly49H$^-$ cells, overt cellular phenotypes showed minimal differences between licensed and unlicensed NK cells (Figure 6a). PCA confirmed that Ly49I$^+$ and Ly49I$^-$ populations became more similar to one another at all timepoints post-infection compared to pre-infection, regardless of Ly49H status (Figure 6b,c). However, the extent and duration of that similarity did differ between Ly49H$^+$ and Ly49H$^-$ cells. Non-antigen specific Ly49I$^+$ and Ly49I$^-$ responses peaked in similarity at 4 DPI before beginning to diverge again, while licensed and unlicensed Ly49H$^+$ NK cells continued to increase in resemblance through 7 DPI and remained highly similar into the memory phase (Figure 6c). The separation that developed between licensed and unlicensed cells in the Ly49H$^-$ compartment could be at least partially attributed to a disproportionate influx of newly generated naive KLRG1$^-$ Ly6C$^-$ cells between licensed and unlicensed cells, whereas the Ly49H$^+$ subsets maintained a similar balance (Figure 6d).

Ultimately, there were very few differences in phenotype between Ly49I$^+$ and Ly49I$^-$ cells during the response. Some of these carried over from the steady-state, such as the continued higher expression of NKp46 and NKG2D on licensed NK cells. The remaining inequalities were evident at singular time points, with nearly all occurring at 4 DPI. These differences at 4 DPI were in Ly49H, Ly49D, IL18Ra, and CD69 (Figure 7a). Specifically, selection for higher avidity Ly49H$^+$ NK cell clones was already evident in licensed NK cells at 4 DPI, but not in unlicensed NK cells; unlicensed cells instead had a slight increase in frequency of Ly49D$^-$ Ly49H$^+$ NK cells. IL18Ra was more significantly downregulated on Ly49I$^+$ NK cells, and especially on Ly49I$^+$ Ly49H$^-$ NK cells. And both Ly49H$^+$ and Ly49H$^-$ Ly49I$^+$ cells displayed higher cell surface expression for the early-activation marker CD69 than their Ly49I$^-$ counterparts. These observations of licensed NK cells were true only for Ly49I$^+$ NK cells and not Ly49C$^+$ NK cells. Ly49C$^+$ Ly49I$^-$ cells tracked more closely in differentiation status with unlicensed cells than Ly49I$^+$ cells (Figure 7b,c), and expanded to a similar magnitude as unlicensed Ly49H$^+$ NK cells during infection (Figure 7d). Though

ostensibly surprising, these results were in actuality consistent with other work that found *cis* interactions between inhibitory Ly49s and MHC-I weakens or ablates the effects of that Ly49 on NK cell function (48, 55). Lastly, one additional difference observed between Ly49I$^+$ and Ly49I$^-$ cells was in CD16 expression at the memory timepoint (35 DPI). A small, but significant, percentage of Ly49I$^-$ NK cells downregulated expression of CD16, while no significant change was seen in the Ly49I$^+$ NK cells (Figure 7e).

The phenotypes of pemNK cells and MCMV-specific mNK cells are highly similar

The unlicensed mNK cell population expanded more than 4-fold from 2.7% of Group 1 ILCs pre-infection to 11.8% post-infection, while the licensed Ly49I$^+$ mNK population only increased by 1.25-fold (Figure 5c). Because the CD16 phenotype at 35 DPI was predominant in unlicensed cells (Figure 7e), we examined whether the two findings were interrelated. Indeed, the CD16$^-$ phenotype revealed itself within the unlicensed KLRG1$^+$ Ly6C$^+$ mNK cell population (Figure 8a). The Ly49I$^-$ KLRG1$^-$ Ly6C$^+$ population also appeared to have more CD16$^-$ cells, however, the difference was non-significant. The licensed CD16$^+$ mNK cells also decreased in frequency compared to uninfected mice, implying that the development of a CD16$^-$ mNK population is not prevented by licensing. However, there was clear favoritism for the unlicensed NK cells. Whether *cis*- or *trans*-interactions between inhibitory Ly49 molecules and MHC-I affect the formation of the small CD16$^-$ subset remains an outstanding question.

This unequal distribution of CD16$^-$ cells in licensed versus unlicensed mNK cells prompted further scrutinization of the memory populations for other changes. While we confirmed that the CD16 phenotype was the major difference between the Ly49I$^+$ and Ly49I$^-$ subsets, other significant observations were recorded. Most of the phenotypes identified on pemNK in naïve mice (Figure 3f) were also present on all KLRG1$^+$ Ly6C$^+$ cells after MCMV infection, occasionally becoming slightly more exaggerated such as in CD49b, CD132, IFNAR, and IL18Ra (Figure 8b). The Ly49H$^-$ NK cells post-infection fully recapitulated the pemNK phenotypes observed in naïve mice. Post-infection Ly49H$^+$ mNK cells, however, no longer expressed less CD96 and NK1.1 compared to naïve cells, and also developed three new memory cell-associated phenotypes. These were an increased MSI of Ly49H, a loss of DNAM-1, and a decrease in NKR-P1B frequency, all of which are consistent with previous characterizations of MCMV-specific NK cell memory (29, 52, 56).

Licensed and unlicensed responses to MCMV converge regardless of specific recognition of MCMV-infected cells

In mice lacking the Ly49H receptor, the absence of an antigen-specific NK cell response during primary MCMV infection is known to affect inflammatory cytokine production and splenic dendritic cell abundances (57), both of which can critically impact NK cell maturation and function (58–60). Moreover, that the Ly49H$^+$ Ly49I$^+$ mNK cells resembled the Ly49H$^+$ Ly49I$^-$ population, more so than the Ly49H$^-$ Ly49I$^+$ subset (Figure 8b), suggested that signaling through Ly49H might obscure any differences in licensed and unlicensed NK cells responses to a viral infection. We, therefore, investigated responses in mice lacking the Ly49H receptor. *Klra8*$^{-/-}$ (Ly49H-deficient) B6 mice were infected alongside wild-type B6 mice and analyzed with an updated mass cytometry panel (Panel

2). Because mice lacking Ly49H are more susceptible to MCMV, the Ly49H-deficient B6 mice received 1/1000th the dose given to wild-type B6. This yielded a similar, though still approximately 2-fold higher viral load, in Ly49H-deficient mice at 7 DPI (Supplementary Figure 4) and prevented excessive splenic tissue destruction. Observations of responses in wild-type B6 mice made previously were confirmed with the updated panel, including superior resolution of the NK1.1$^{lo/-}$ CD16^{-} population at 4 DPI (Figure 9a,b, metaclusters B and C). The new panel also included the checkpoint receptors TIGIT and LAG-3, which, like PD-1 (Figure 6a), were not found on any mNK populations (metaclusters M and N).

Although the Ly49H-deficient mice exhibited a clearly distinct response from wild-type mice (Figure 9a,b), licensed and unlicensed cells within the non-antigen specific NK cell response still converged just as in wild-type mice (Figure 9c). The pattern of their relationship closely mirrored that of Ly49H^{-} NK cells in wild-type mice, with the notable exception of Ly49I^{+} and Ly49I^{-} cells in Ly49H-deficient mice becoming more dissimilar at 28 DPI than they were in uninfected mice. We attribute this to the much higher frequency of KLRG1^{-} Ly6C^{-} NK cells in Ly49H-deficient mice, and a corresponding reduced frequency of Ly49I^{+} and KLRG1^{+} Ly6C^{+} cells (Figure 9d). This distribution weighted towards undifferentiated NK cells likely reflected a more limited history of pathogen exposure, similar to how NK cell diversity in humans varies according to their histories of viral infections (61).

Consistent with the NK cells from wild-type mice, only select few differences between licensed and unlicensed cells were observed in Ly49H-deficient mice. Altered phenotypes in IL18Ra, CD69, and Ly49D at 4 DPI appeared in the Ly49H-deficient mice just as they did in wild-type mice, though Ly49I^{+} cells from Ly49H-deficient mice now also saw an uptick in the frequency of Ly49D^{+} NK cells in addition to the downregulation in the frequency of Ly49D^{+} NK cells within the Ly49I^{-} subset (Figure 9e). In contrast to the wild-type cells though, a CD16^{-} memory population did not appear in Ly49H-deficient mice (Figure 9f). Considering the CD16^{-} cells were concentrated in the unlicensed mNK Ly49H^{+} population in wild-type mice and that population did not significantly expand in Ly49H-deficient mice (Figure 9a, metacluster N), this was not altogether surprising. In summary, regardless of whether an antigen-specific NK cell response to MCMV was generated, the licensed and unlicensed NK cell responses converged upon a singular phenotype. The dominance of the unlicensed response, therefore, does not appear to be the result of any functional deficiencies we could observe by phenotyping, but rather because of the combined effects of inhibitory signaling on proliferation and a smaller pool of KLRG1^{-} Ly6C^{-} Ly49I^{+} NK cells at the time of infection.

Discussion

In B6 mice, the NK cell compartment can be separated into licensed cells, which are Ly49C^{+} and/or Ly49I^{+}, and unlicensed cells, which lack both of those receptors (14, 26). Under non-inflammatory conditions licensed cells show superior functional activity *in vitro*, especially when presented with MHC class I-deficient target cells (15, 62, 63). Following exposure to inflammatory cytokines, however, unlicensed cells become equally functional to and, in at least some cases, better effectors than their licensed equivalents (14, 15, 17).

One such example is in MCMV infection of B6 mice (17). SHP-1 recruitment following inhibitory Ly49 ligand recognition limits proliferation via Vav1 dephosphorylation (18), and consequently the ability of licensed NK cells to provide an optimal immune response to the virus (17). Given Vav1 has a much more extensive role in NK cell activation than just fostering proliferation (23–25), we developed and implemented a mass cytometry panel to further investigate whether licensed and unlicensed NK cell responses to MCMV were qualitatively different beyond their proliferation efficiencies.

At steady-state, splenic NK cells separated into five major subsets according to their expression of the differentiation markers KLRG1 and Ly6C, with the additional separation of KLRG1^{-} Ly6C^{-} cells into CD90^{hi} and CD90$^{lo/-}$ subsets. Despite approximately half of all cells expressing Ly49C and/or Ly49I, the licensed and unlicensed cells were not evenly distributed among the five KLRG1/Ly6C/CD90 subsets. Unlicensed cells were much more frequently KLRG1^{-} than KLRG1^{+}, while licensed cells were the opposite. Antigen-experienced KLRG1^{+} NK cells are known to be less proliferative than naïve cells, regardless of licensing status (41, 50). Moreover, a significant proportion of Ly49I^{+} cells in naïve mice had the KLRG1^{+} Ly6C^{+} phenotype closely resembling MCMV-specific mNK cells, and mNK cells are refractory to heterologous stimuli (43, 44). These pre-existing KLRG1^{+} Ly6C^{+} NK cells in naïve mice closely resembled *bona-fide* MCMV-specific mNK cells in phenotype, having downregulated cytokine (e.g. CD132, IFNAR, IL18Ra) and co-stimulatory (e.g. CD2, CD11a) receptors, and similarly showed less responsiveness to cytokine stimulation *in vitro*. We, therefore, conclude that unlicensed NK cells dominate the response not only because their ability to proliferate is unrestricted by an inhibitory Ly49, but also because many licensed NK cells in naïve mice are already differentiated into KLRG1^{+} Ly6C^{-} and KLRG1^{+} Ly6C^{+} NK cells that have an inherent reduced ability to proliferate and respond to unrelated immunological stimuli.

The dissimilarities between Ly49I^{+} and Ly49I^{-} NK cell phenotypes, after accounting for differentiation status, further argued against licensed cells being at a disadvantage beyond the restrictions inhibitory Ly49 signaling places on proliferation. KLRG1^{-} Ly6C^{-} Ly49I^{+} NK cells in naïve mice actually had a phenotype predictive of a *more* potent response. They expressed more of the activating receptors Ly49H, NKG2D, and NKp46, and less of the inhibitory NKR-P1B than their Ly49I^{-} equivalents. Moreover, Ly49I^{+} cells had a more activated phenotype at 4 DPI; selection for Ly49H^{hi} NK cell clones was already occurring, surface density of CD69 was higher, and IL18Ra downregulation was more substantial. A model of hematopoietic stem cell transplantation and MCMV infection similarly found the kinetics of the licensed NK cell response outpaces that of the unlicensed response (64). Interestingly, in the absence of Ly49H, licensed cells exhibited an increase in Ly49D expression, another activating NKR that nonetheless lacks a ligand in this model. Combined with the observed higher expression of Ly49H on licensed cells in naive mice, these data suggest licensed NK cells might upregulate the signaling adaptor DAP12, the primary partner for Ly49H and Ly49D surface expression (65), or alternatively select for NK cell clones already expressing higher amounts of Ly49H. The functional potency of licensed NK cells is proportional to the amount of inhibitory receptor expressed (62, 63), so selection for cells with higher DAP12 expression instead of lower Ly49I expression would ostensibly yield NK cells better capable of cytokine production and target cell killing. Unlicensed

cells, on the other hand, need only select for clones in which there is less Ly49D, since there is no check on DAP12 signaling from inhibitory Ly49, but because Ly49D may act as a competitive inhibitor of Ly49H for DAP12. Regardless, the overall similarities in phenotype suggested that there was no apparent difference in licensed and unlicensed NK cell responses beyond the previously observed effect on proliferation magnitude (17). Moreover, we show here that observation is applicable only to licensing receptors that do not interact with their ligands in *cis*, a result consistent with other studies that have found *cis*-interactions stymie the inhibitory effect of Ly49A (55) and Ly49C (48). We also note that the minimal differences in licensed and unlicensed NK cell responses occurred in a model in which activating and inhibitory NKRs were not competing with one another for a ligand. The impact of licensing NKRs in such a scenario may be even less pronounced. This could be investigated in MA/My mice, in which the activating receptor Ly49P confers resistance to MCMV via an interaction with H2-K^d (66), an MHC-I allele recognized by the inhibitory Ly49G and Ly49O receptors present in MA/My mice (67).

Ly49I also failed to impact the generation of MCMV-specific mNK cells. $Ly49H^+$ $Ly49I^+$ and $Ly49H^+$ $Ly49I^-$ mNK were indistinguishable except for a small pool of $CD16^-$ cells occurring preferentially in the unlicensed group. The $Ly49H^-$ memory-like NK cells after infection recovered the same phenotype present on pemNK cells, and these $Ly49H^-$ memory-like populations had significant differences in only CD96, NK1.1, and DNAM-1 expression when compared to the MCMV-specific mNK cells. That the $Ly49I^+$ $Ly49H^+$ cells took on the phenotype of the unlicensed $Ly49H^+$ NK cells rather than the licensed $Ly49H^-$ NK cells further argued that the influence of Ly49H on NK cell memory differentiation superseded any effect signaling via inhibitory Ly49s might have caused on the memory response.

Regarding the $CD16^-$ population in the mNK cell subset at 35 DPI, it was curiously the second $CD16^-$ population to develop during the infection. The first appeared at 4 DPI, although the likelihood this first population and the one found post-infection are related is low. Not only did the population at 4 DPI disappear before the peak of the NK cell response, but there were other observations to distinguish them. Specifically, the 4 DPI population was $NK1.1^{lo/-}$, while the mNK cells retained full NK1.1 expression. Additionally, the subset at 4 DPI appeared in both wild-type and Ly49H-deficient mice, but the $CD16^-$ memory-like NK cell population did not develop in Ly49H-deficient mice. And lastly, the $CD16^-$ population at 4 DPI was near evenly split between $Ly49I^+$ and $Ly49I^-$, while the mNK population was decisively more abundant in the unlicensed population. Considering stimulation of NK cells from B6 mice via CD16 is weak (68), it is unclear why such a population would develop or what advantages it might offer in the event of MCMV reactivation or reinfection.

In conclusion, based on the in-depth analysis of NK cells throughout the expansion, contraction, and memory phases of the response to MCMV, licensed NK cells are disadvantaged compared to unlicensed NK cells in B6 mice by two properties: a restriction on proliferation due to inhibitory Ly49 signaling resulting from ligand recognition *in trans*, and a smaller pool of readily responsive $KLRG1^-$ $Ly6C^-$ NK cells. Future investigations should examine whether these differences extend to other viral infections and/or oncogenic

events, as well as the extent to which pathogen exposure history impacts the NK cell response to novel immune challenges.

Supplementary Material

Refer to Web version on PubMed Central for supplementary material.

Acknowledgments

Grant support

We acknowledge the PFCC (RRID:SCR_018206) supported in part by NIH P30 DK063720 and by the NIH S10 Instrumentation Grant S10 1S10OD018040-01. O.A.A. holds a PostDoctoral Enrichment Program Award from the Burroughs Wellcome Fund (BWF) and is a Cancer Research Institute Irvington Fellow supported by the Cancer Research Institute (CRI). O.A.A., M.D.R.G.-H., and L.L.L. are supported by the Parker Institute for Cancer Immunotherapy (PICI) and by NIH grants AI068129 and AI146581.

Abbreviations

B6	C57BL/6
DPI	Days Post-Infection
ILC	Innate Lymphoid Cell
MCMV	Mouse Cytomegalovirus
mNK	memory Natural Killer
MSI	Mean Signal Intensity
NK	Natural Killer
NKR	Natural Killer cell Receptor
PCA	Principal Component Analysis
pemNK	pre-existing memory-like Natural Killer
PFU	Plaque Forming Units

References

1. Sun JC, and Lanier LL. 2011. NK cell development, homeostasis and function: parallels with CD8+ T cells. Nat Rev Immunol 11: 645–657. [PubMed: 21869816]
2. Lanier LL 2008. Up on the tightrope: natural killer cell activation and inhibition. Nat Immunol 9: 495–502. [PubMed: 18425106]
3. Raulet DH 2006. Missing self recognition and self tolerance of natural killer (NK) cells. Semin Immunol 18: 145–150. [PubMed: 16740393]
4. Held W, and Kunz B. 1998. An allele-specific, stochastic gene expression process controls the expression of multiple Ly49family genes and generates a diverse, MHC-specific NK cell receptor repertoire. Eur J Immunol 28: 2407–2416. [PubMed: 9710218]
5. Smith HRC, Chuang HH, Wang LL, Salcedo M, Heusel JW, and Yokoyama WM. 2000. Nonstochastic Coexpression of Activation Receptors on Murine Natural Killer Cells. J Exp Medicine 191: 1341–1354.

6. Millan AJ, Hom BA, Libang JB, Sindi S, and Manilay JO. 2021. Evidence for Prescribed NK Cell Ly-49 Developmental Pathways in Mice. J Immunol 206: 1215–1227. [PubMed: 33495236]
7. Carlyle JR, Mesci A, Fine JH, Chen P, Bélanger S, Tai L-H, and Makrigiannis AP. 2008. Evolution of the Ly49 and Nkrp1 recognition systems. Semin Immunol 20: 321–330. [PubMed: 18595730]
8. Held W, and Raulet DH. 1997. Expression of the Ly49A gene in murine natural killer cell clones is predominantly but not exclusively mono-allelic. Eur J Immunol 27: 2876–2884. [PubMed: 9394813]
9. Rouhi A, Gagnier L, Takei F, and Mager DL. 2006. Evidence for Epigenetic Maintenance of Ly49a Monoallelic Gene Expression. J Immunol 176: 2991–2999. [PubMed: 16493057]
10. Rouhi A, Lai CB, Cheng TP, Takei F, Yokoyama WM, and Mager DL. 2009. Evidence for high bi-allelic expression of activating Ly49 receptors. Nucleic Acids Res 37: 5331–5342. [PubMed: 19605564]
11. Sun JC, and Lanier LL. 2008. Tolerance of NK cells encountering their viral ligand during development. J Exp Medicine 205: 1819–1828.
12. Lopez-Vergès S, Milush JM, Schwartz BS, Pando MJ, Jarjoura J, York VA, Houchins JP, Miller S, Kang S-M, Norris PJ, Nixon DF, and Lanier LL. 2011. Expansion of a unique CD57+NKG2Chi natural killer cell subset during acute human cytomegalovirus infection. Proc National Acad Sci 108: 14725–14732.
13. Horowitz A, Strauss-Albee DM, Leipold M, Kubo J, Nemat-Gorgani N, Dogan OC, Dekker CL, Mackey S, Maecker H, Swan GE, Davis MM, Norman PJ, Guethlein LA, Desai M, Parham P, and Blish CA. 2013. Genetic and Environmental Determinants of Human NK Cell Diversity Revealed by Mass Cytometry. Sci Transl Med 5: 208ra145–208ra145.
14. Kim S, Poursine-Laurent J, Truscott SM, Lybarger L, Song Y-J, Yang L, French AR, Sunwoo JB, Lemieux S, Hansen TH, and Yokoyama WM. 2005. Licensing of natural killer cells by host major histocompatibility complex class I molecules. Nature 436: 709–713. [PubMed: 16079848]
15. Fernandez NC, Treiner E, Vance RE, Jamieson AM, Lemieux S, and Raulet DH. 2005. A subset of natural killer cells achieves self-tolerance without expressing inhibitory receptors specific for self-MHC molecules. Blood 105: 4416–4423. [PubMed: 15728129]
16. Orr MT, and Lanier LL. 2010. Natural Killer Cell Education and Tolerance. Cell 142: 847–856. [PubMed: 20850008]
17. Orr MT, Murphy WJ, and Lanier LL. 2010. “Unlicensed” natural killer cells dominate the response to cytomegalovirus infection. Nat Immunol 11: 321–327. [PubMed: 20190757]
18. Stebbins CC, Watzl C, Billadeau DD, Leibson PJ, Burshtyn DN, and Long EO. 2003. Vav1 Dephosphorylation by the Tyrosine Phosphatase SHP-1 as a Mechanism for Inhibition of Cellular Cytotoxicity. Mol Cell Biol 23: 6291–6299. [PubMed: 12917349]
19. Mahmoud AB, Tu MM, Wight A, Zein HS, Rahim MMA, Lee S-H, Sekhon HS, Brown EG, and Makrigiannis AP. 2016. Influenza Virus Targets Class I MHC-Educated NK Cells for Immunoevasion. Plos Pathog 12: e1005446. [PubMed: 26928844]
20. Binstadt BA, Brumbaugh KM, Dick CJ, Scharenberg AM, Williams BL, Colonna M, Lanier LL, Kinet J-P, Abraham RT, and Leibson PJ. 1996. Sequential Involvement of Lck and SHP-1 with MHC-Recognizing Receptors on NK Cells Inhibits FcR-Initiated Tyrosine Kinase Activation. Immunity 5: 629–638. [PubMed: 8986721]
21. Nakamura MC, Niemi EC, Fisher MJ, Shultz LD, Seaman WE, and Ryan JC. 1997. Mouse Ly-49A Interrupts Early Signaling Events in Natural Killer Cell Cytotoxicity and Functionally Associates with the SHP-1 Tyrosine Phosphatase. J Exp Medicine 185: 673–684.
22. Tarakhovsky A, Turner M, Schaal S, Mee PJ, Duddy LP, Rajewsky K, and Tybulewicz VLJ. 1995. Defective antigen receptor-mediated proliferation of B and T cells in the absence of Vav. Nature 374: 467–470. [PubMed: 7700358]
23. Billadeau DD, Brumbaugh KM, Dick CJ, Schoon RA, Bustelo XR, and Leibson PJ. 1998. The Vav–Rac1 Pathway in Cytotoxic Lymphocytes Regulates the Generation of Cell-mediated Killing. J Exp Medicine 188: 549–559.
24. Chan G, Hanke T, and Fischer K. 2001. Vav-1 regulates NK T cell development and NK cell cytotoxicity. Eur J Immunol 31: 2403–2410. [PubMed: 11500824]

25. Colucci F, Rosmaraki E, Bregenholt S, Samson SI, Bartolo VD, Turner M, Vanes L, Tybulewicz V, and Santo JPD. 2001. Functional Dichotomy in Natural Killer Cell Signaling. J Exp Medicine 193: 1413–1424.
26. Hanke T, Takizawa H, McMahon CW, Busch DH, Pamer EG, Miller JD, Altman JD, Liu Y, Cado D, Lemonnier FA, Bjorkman PJ, and Raulet DH. 1999. Direct Assessment of MHC Class I Binding by Seven Ly49 Inhibitory NK Cell Receptors. Immunity 11: 67–77. [PubMed: 10435580]
27. Arase H, Mocarski ES, Campbell AE, Hill AB, and Lanier LL. 2002. Direct Recognition of Cytomegalovirus by Activating and Inhibitory NK Cell Receptors. Science 296: 1323–1326. [PubMed: 11950999]
28. Smith HRC, Heusel JW, Mehta IK, Kim S, Dorner BG, Naidenko OV, Iizuka K, Furukawa H, Beckman DL, Pingel JT, Scalzo AA, Fremont DH, and Yokoyama WM. 2002. Recognition of a virus-encoded ligand by a natural killer cell activation receptor. Proc National Acad Sci 99: 8826–8831.
29. Sun JC, Beilke JN, and Lanier LL. 2009. Adaptive immune features of natural killer cells. Nature 457: 557–561. [PubMed: 19136945]
30. Iizuka K, Naidenko OV, Plougastel BFM, Fremont DH, and Yokoyama WM. 2003. Genetically linked C-type lectin-related ligands for the NKRP1 family of natural killer cell receptors. Nat Immunol 4: 801–807. [PubMed: 12858173]
31. MacFarlane AW, Yamazaki T, Fang M, Sigal LJ, Kurosaki T, and Campbell KS. 2008. Enhanced NK-cell development and function in BCAP-deficient mice. Blood 112: 131–140. [PubMed: 18337558]
32. Zunder ER, Finck R, Behbehani GK, Amir ED, Krishnaswamy S, Gonzalez VD, Lorang CG, Bjornson Z, Spitzer MH, Bodenmiller B, Fantl WJ, Pe'er D, and Nolan GP. 2015. Palladium-based mass tag cell barcoding with a doublet-filtering scheme and single-cell deconvolution algorithm. Nat Protoc 10: 316–333. [PubMed: 25612231]
33. Finck R, Simonds EF, Jager A, Krishnaswamy S, Sachs K, Fantl W, Pe'er D, Nolan GP, and Bendall SC. 2013. Normalization of mass cytometry data with bead standards. Cytom Part A 83A: 483–494.
34. Kotecha N, Krutzik PO, and Irish JM. 2010. Web-Based Analysis and Publication of Flow Cytometry Experiments. Curr Protoc Cytom 53: 10.17.1–10.17.24.
35. Amir ED, Davis KL, Tadmor MD, Simonds EF, Levine JH, Bendall SC, Shenfeld DK, Krishnaswamy S, Nolan GP, and Pe'er D. 2013. viSNE enables visualization of high dimensional single-cell data and reveals phenotypic heterogeneity of leukemia. Nat Biotechnol 31: 545–552. [PubMed: 23685480]
36. Gassen SV, Callebaut B, Helden MJV, Lambrecht BN, Demeester P, Dhaene T, and Saeys Y. 2015. FlowSOM: Using self-organizing maps for visualization and interpretation of cytometry data. Cytom Part A 87: 636–645.
37. Kamimura Y, and Lanier LL. 2015. Homeostatic Control of Memory Cell Progenitors in the Natural Killer Cell Lineage. Cell Reports 10: 280–291. [PubMed: 25578733]
38. Spits H, Bernink JH, and Lanier L. 2016. NK cells and type 1 innate lymphoid cells: partners in host defense. Nat Immunol 17: 758–764. [PubMed: 27328005]
39. Weizman O-E, Adams NM, Schuster IS, Krishna C, Pritykin Y, Lau C, Degli-Esposti MA, Leslie CS, Sun JC, and O'Sullivan TE. 2017. ILC1 Confer Early Host Protection at Initial Sites of Viral Infection. Cell 171: 795–808.e12. [PubMed: 29056343]
40. Meininger I, Carrasco A, Rao A, Soini T, Kokkinou E, and Mjösberg J. 2020. Tissue-Specific Features of Innate Lymphoid Cells. Trends Immunol 41: 902–917. [PubMed: 32917510]
41. Huntington ND, Tabarias H, Fairfax K, Brady J, Hayakawa Y, Degli-Esposti MA, Smyth MJ, Tarlinton DM, and Nutt SL. 2007. NK Cell Maturation and Peripheral Homeostasis Is Associated with KLRG1 Up-Regulation. J Immunol 178: 4764–4770. [PubMed: 17404256]
42. Chiossone L, Chaix J, Fuseri N, Roth C, Vivier E, and Walzer T. 2009. Maturation of mouse NK cells is a 4-stage developmental program. Blood 113: 5488–5496. [PubMed: 19234143]
43. Min-Oo G, and Lanier LL. 2014. Cytomegalovirus generates long-lived antigen-specific NK cells with diminished bystander activation to heterologous infection. J Exp Med 211: 2669–2680. [PubMed: 25422494]

44. Nabekura T, and Lanier LL. 2016. Tracking the fate of antigen-specific versus cytokine-activated natural killer cells after cytomegalovirus infection. J Exp Med 213: 2745–2758. [PubMed: 27810928]
45. Rex DAB, Agarwal N, Prasad TSK, Kandasamy RK, Subbannayya Y, and Pinto SM. 2020. A comprehensive pathway map of IL-18-mediated signalling. J Cell Commun Signal 14: 257–266. [PubMed: 31863285]
46. Kalina U, Kauschat D, Koyama N, Nuernberger H, Ballas K, Koschmieder S, Bug G, Hofmann W-K, Hoelzer D, and Ottmann OG. 2000. IL-18 Activates STAT3 in the Natural Killer Cell Line 92, Augments Cytotoxic Activity, and Mediates IFN-γ Production by the Stress Kinase p38 and by the Extracellular Regulated Kinases p44erk-1 and p42erk-21. J Immunol 165: 1307–1313. [PubMed: 10903731]
47. Wight A, Mahmoud AB, Scur M, Tu MM, Rahim MMA, Sad S, and Makrigiannis AP. 2018. Critical role for the Ly49 family of class I MHC receptors in adaptive natural killer cell responses. Proc National Acad Sci 115: 201722374.
48. Forbes CA, Scalzo AA, Degli-Esposti MA, and Coudert JD. 2014. Ly49C-Dependent Control of MCMV Infection by NK Cells Is Cis-Regulated by MHC Class I Molecules. Plos Pathog 10: e1004161. [PubMed: 24873973]
49. Scarpellino L, Oeschger F, Guillaume P, Coudert JD, Lévy F, Leclercq G, and Held W. 2007. Interactions of Ly49 Family Receptors with MHC Class I Ligands in trans and cis. J Immunol 178: 1277–1284. [PubMed: 17237373]
50. Kamimura Y, and Lanier LL. 2015. Homeostatic Control of Memory Cell Progenitors in the Natural Killer Cell Lineage. Cell Reports 10: 280–291. [PubMed: 25578733]
51. Negi S, Das DK, Pahari S, Nadeem S, and Agrewala JN. 2019. Potential Role of Gut Microbiota in Induction and Regulation of Innate Immune Memory. Front Immunol 10: 2441. [PubMed: 31749793]
52. Aguilar OA, Berry R, Rahim MMA, Reichel JJ, Popović B, Tanaka M, Fu Z, Balaji GR, Lau TNH, Tu MM, Kirkham CL, Mahmoud AB, Mesci A, Krmpotić A, Allan DSJ, Makrigiannis AP, Jonjić S, Rossjohn J, and Carlyle JR. 2017. A Viral Immunoevasin Controls Innate Immunity by Targeting the Prototypical Natural Killer Cell Receptor Family. Cell 169: 58–71.e14. [PubMed: 28340350]
53. Hwang I, Zhang T, Scott JM, Kim AR, Lee T, Kakarla T, Kim A, Sunwoo JB, and Kim S. 2012. Identification of human NK cells that are deficient for signaling adaptor FcRγ and specialized for antibody-dependent immune functions. Int Immunol 24: 793–802. [PubMed: 22962434]
54. Zhang T, Scott JM, Hwang I, and Kim S. 2013. Cutting Edge: Antibody-Dependent Memory-like NK Cells Distinguished by FcRγ Deficiency. J Immunol 190: 1402–1406. [PubMed: 23345329]
55. Doucey M-A, Scarpellino L, Zimmer J, Guillaume P, Luescher IF, Bron C, and Held W. 2004. Cis association of Ly49A with MHC class I restricts natural killer cell inhibition. Nat Immunol 5: 328–336. [PubMed: 14973437]
56. Nabekura T, Kanaya M, Shibuya A, Fu G, Gascoigne NRJ, and Lanier LL. 2014. Costimulatory Molecule DNAM-1 Is Essential for Optimal Differentiation of Memory Natural Killer Cells during Mouse Cytomegalovirus Infection. Immunity 40: 225–234. [PubMed: 24440149]
57. Mitrović M, Arapović J, Jordan S, Fodil-Cornu N, Ebert S, Vidal SM, Krmpotić A, Reddehase MJ, and Jonjić S. 2012. The NK Cell Response to Mouse Cytomegalovirus Infection Affects the Level and Kinetics of the Early CD8+ T-Cell Response. J Virol 86: 2165–2175. [PubMed: 22156533]
58. Abel AM, Yang C, Thakar MS, and Malarkannan S. 2018. Natural Killer Cells: Development, Maturation, and Clinical Utilization. Front Immunol 9: 1869. [PubMed: 30150991]
59. Madera S, Rapp M, Firth MA, Beilke JN, Lanier LL, and Sun JC. 2016. Type I IFN promotes NK cell expansion during viral infection by protecting NK cells against fratricide. J Exp Med 213: 225–233. [PubMed: 26755706]
60. Marcenaro E, Carlomagno S, Pesce S, Moretta A, and Sivori S. 2011. Current Topics in Innate Immunity II. Adv Exp Med Biol 946: 295–308.
61. Strauss-Albee DM, Fukuyama J, Liang EC, Yao Y, Jarrell JA, Drake AL, Kinuthia J, Montgomery RR, John-Stewart G, Holmes S, and Blish CA. 2015. Human NK cell repertoire diversity reflects immune experience and correlates with viral susceptibility. Sci Transl Med 7: 297ra115–297ra115.

62. Joncker NT, Fernandez NC, Treiner E, Vivier E, and Raulet DH. 2009. NK Cell Responsiveness Is Tuned Commensurate with the Number of Inhibitory Receptors for Self-MHC Class I: The Rheostat Model. J Immunol 182: 4572–4580. [PubMed: 19342631]

63. Brodin P, Lakshmikanth T, Johansson S, Kärre K, and Höglund P. 2009. The strength of inhibitory input during education quantitatively tunes the functional responsiveness of individual natural killer cells. Blood 113: 2434–2441. [PubMed: 18974374]

64. Sungur CM, Tang-Feldman YJ, Ames E, Alvarez M, Chen M, Longo DL, Pomeroy C, and Murphy WJ. 2013. Murine natural killer cell licensing and regulation by T regulatory cells in viral responses. Proc National Acad Sci 110: 7401–7406.

65. Orr MT, Sun JC, Hesslein DGT, Arase H, Phillips JH, Takai T, and Lanier LL. 2009. Ly49H signaling through DAP10 is essential for optimal natural killer cell responses to mouse cytomegalovirus infection. J Exp Med 206: 807–817. [PubMed: 19332875]

66. Kielczewska A, Pyzik M, Sun T, Krmpotic A, Lodoen MB, Munks MW, Babic M, Hill AB, Koszinowski UH, Jonjic S, Lanier LL, and Vidal SM. 2009. Ly49P recognition of cytomegalovirus-infected cells expressing H2-Dk and CMV-encoded m04 correlates with the NK cell antiviral response. J Exp Medicine 206: 515–523.

67. Schenkel AR, Kingry LC, and Slayden RA. 2013. The Ly49 Gene Family. A Brief Guide to the Nomenclature, Genetics, and Role in Intracellular Infection. Front Immunol 4: 90. [PubMed: 23596445]

68. Bergman I, Basse PH, Barmada MA, Griffin JA, and Cheung N-KV. 2000. Comparison of in vitro antibody-targeted cytotoxicity using mouse, rat and human effectors. Cancer Immunol Immunother 49: 259–266. [PubMed: 10941909]

Key Points

- Naïve C57BL/6 mice have a pre-existing memory-like NK cell population
- The pre-existing memory-like population comprises predominantly licensed NK cells
- Ly49I has limited direct effect on NK cell responses to MCMV beyond proliferation

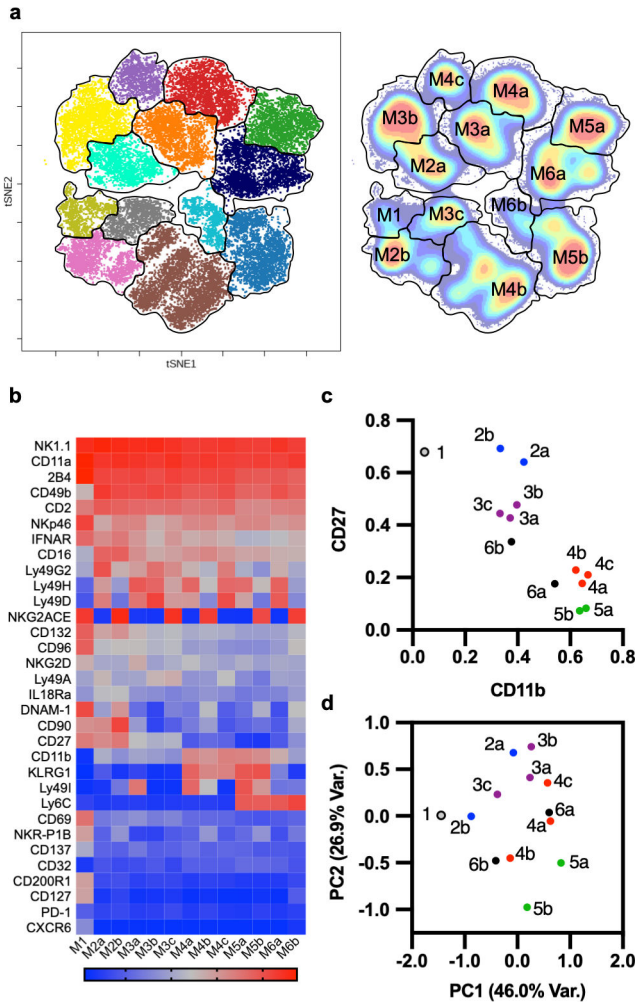

Figure 1.

Steady-state composition of splenic group 1 ILC compartment. (a) viSNE map and associated density plot of splenic group 1 ILCs from uninfected B6 mice ($n = 4$), colored by metacluster. (b) Heatmap displaying the phenotype of each of the 13 metaclusters. Metacluster values represent the weighted average of cluster medians normalized as percentage of global maximum. (c) Maturation status of the group 1 ILC metaclusters according to CD11b and CD27 expression. (d) PCA of metaclusters present in healthy wild-type B6 mice. Data presented is from a single experiment but is consistent with data generated in four total experiments.

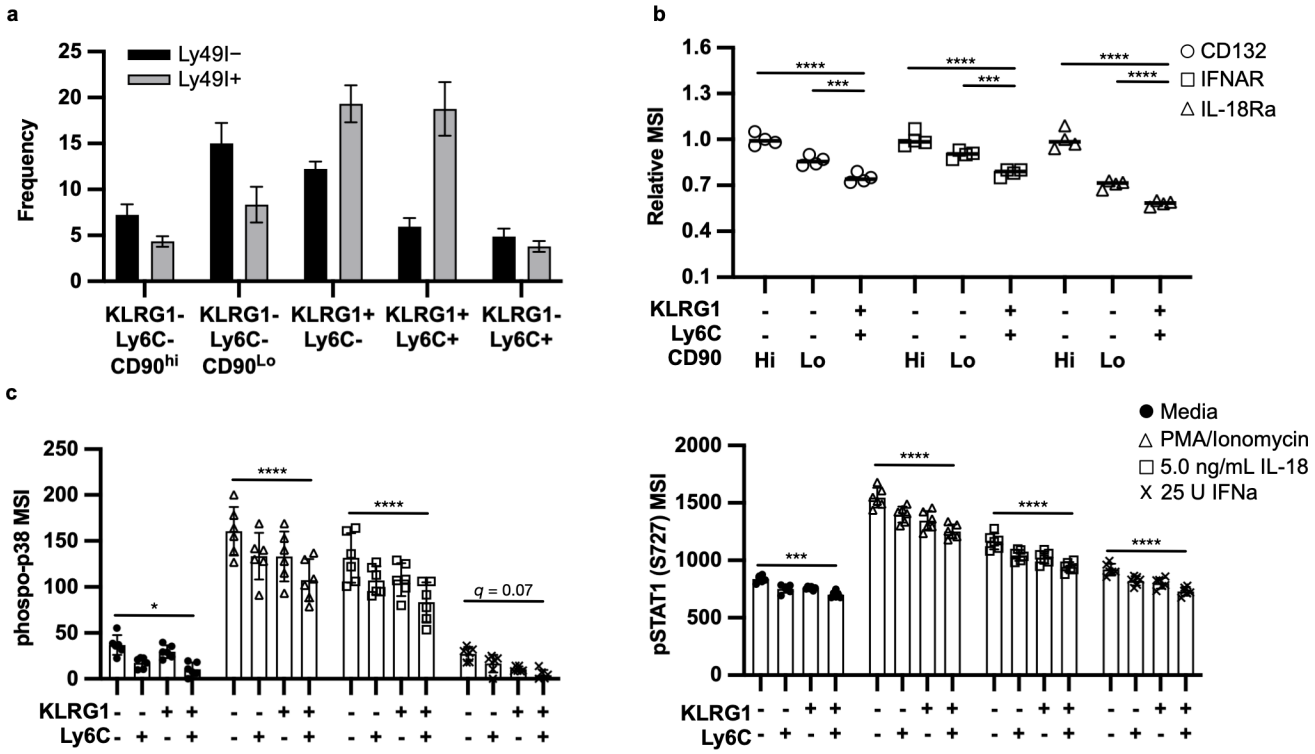

Figure 2.

Most licensed NK cells in uninfected mice have differentiated into less responsive NK cell subsets. (a) Distribution of Ly49I^{+} and Ly49I^{-} NK cells among the five NK cell subsets as a percentage of the total NK cell population. Data collected from four mice in a single CyTOF run but is consistent with data acquired in three additional experiments. (b) Expression of cytokine receptors on immature KLRG1^{-} Ly6C^{-} and fully mature KLRG1^{+} Ly6C^{+} NK cells. Intensity reported relative to KLRG1^{-} Ly6C^{-} CD90^{hi} population. (c) Phosphorylation of p38 and STAT1 in NK cell subsets after treatment with PMA + ionomycin, IL-18, or IFNα. Signal intensity measured by flow cytometry. Data acquired in triplicate. * p <0.05, *** p <0.001, **** p<0.0001, by repeated measures two-way ANOVA for (b) and ordinary two-way ANOVA for (c).

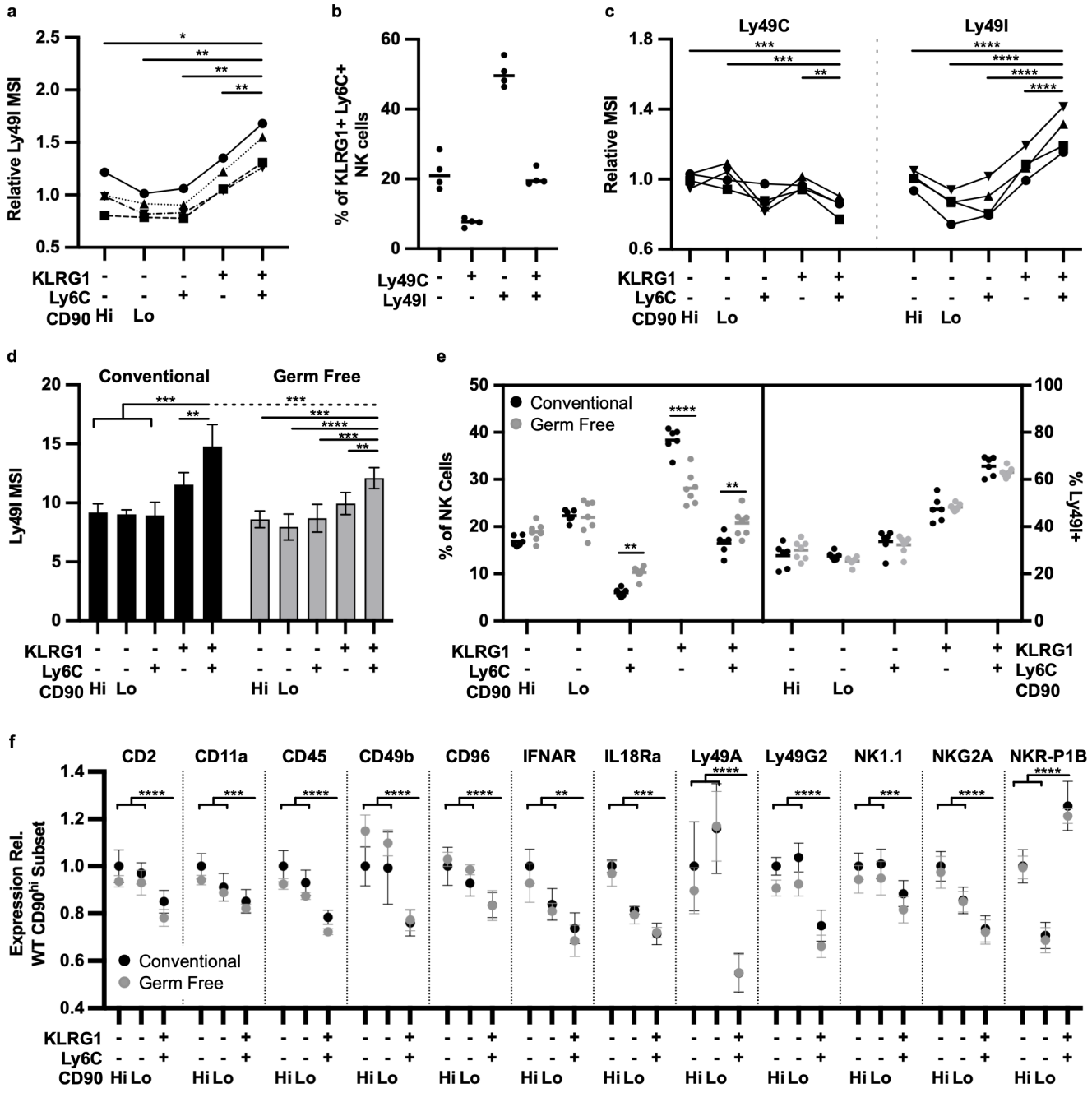

Figure 3.

Pre-existing memory-like NK cells develop in conventionally-housed and germ-free mice (a) Relative mean signal intensity of Ly49I on NK cell subsets as determined by the 5E6 antibody. Data is representative of a single experiment (n = 4), but consistent with analysis of five additional experiments using both CyTOF and flow cytometry. (b) Frequency of Ly49C and Ly49I on KLRG1^{+} Ly6C^{+} NK cells alone or in tandem using Ly49C-specific (clone 4LO331) and Ly49I-specific (YL1–90) antibodies. (c) Relative mean signal intensity of Ly49C and Ly49I on KLRG1+ Ly6C+ NK cells determined with the 4LO331 and YL1–90 antibodies. n =4 mice, experiment repeated in duplicate. (d) Relative mean signal

intensity of Ly49I on splenic NK cells from conventionally housed (n = 6) and germ-free mice (n = 7). Data presented from a single CyTOF run. (e) Distribution of NK cells among the five NK cell subsets (left) and frequency of $Ly49I^{+}$ NK cells within each of those subsets (right). (f) Phenotypic differences between naïve $KLRG1^{-}$ $Ly6C^{-}$ NK cells and pemNK cells, shown as expression intensity relative to $KLRG1^{-}$ $Ly6C^{-}$ $CD90^{hi}$ cells from conventionally-housed mice. ** p <0.01, *** p <0.001, **** p <0.0001

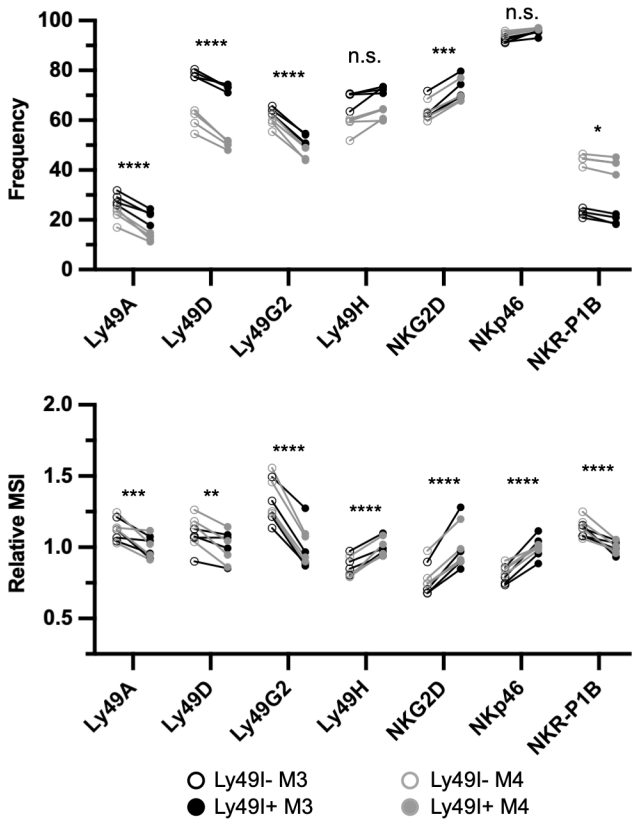

Figure 4.

Licensed and unlicensed NK cells of similar differentiation status have different NKR expression patterns. Expression frequency (top) and mean signal intensity (below) of NKRs on Ly49I^{+} and Ly49I^{-} cells. Intensity measurements reported relative to the MSI of Ly49I^{+} KLRG1^{-} Ly6C^{-} CD90^{lo} cells. Data presented from a single experiment but is representative of three additional CyTOF runs. * p<0.05, ** p <0.01, *** p <0.001, **** p <0.0001.

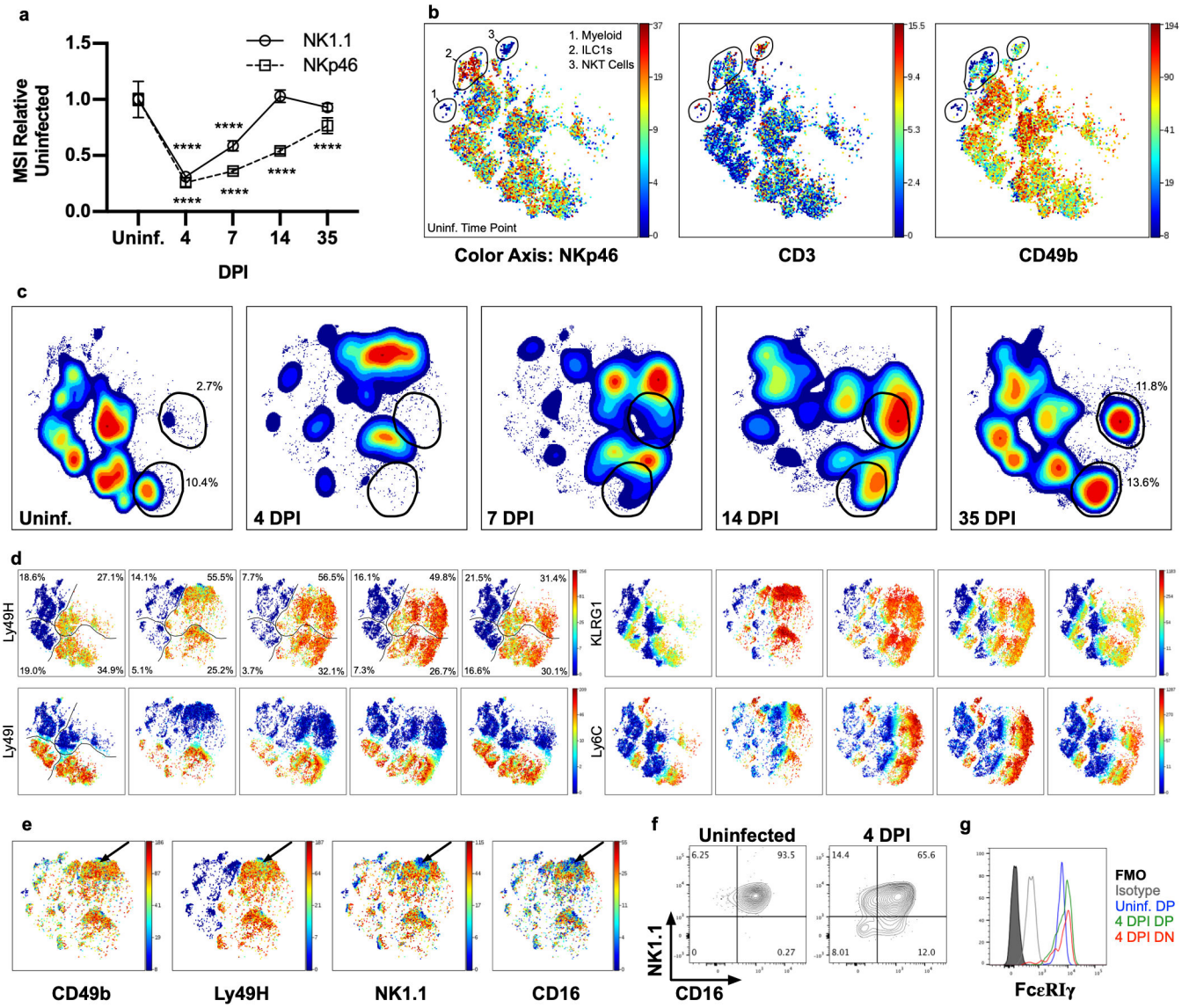

Figure 5.

An alternative gating strategy for group 1 ILCs reveals an NK1.1^{-} CD16^{-} NK cell population at 4 DPI. (a) NK1.1 and NKp46 expression intensities relative to uninfected mice. Data shown from a single experiment but representative of four total. **** p <0.001 (b) Example plot demonstrating the fidelity of a gating strategy for group 1 ILCs that does not make use of NK1.1 or NKp46. Plots are colored according to NKp46 (left), CD3 (middle), and CD49b (right). (c) Density plots showing the dynamic changes in group 1 ILCs during MCMV infection. Gated areas demarcate KLRG1^{+} Ly6C^{+} memory and memory-like populations. (d) Ly49H, Ly49I, KLRG1, and Ly6C expression on group 1 ILCs during MCMV infection. Percentages in the Ly49H plots correspond to the Ly49H^{-} Ly49I^{-} (top left), Ly49H^{-} Ly49I^{+} (bottom left), Ly49H^{+} Ly49I^{-} (top right), and Ly49H^{+} Ly49I^{+} population frequencies at the respective time points. (e) Evidence of a CD49b^{+} Ly49H^{+} NK1.1^{-} CD16^{-} NK cell population (arrow) at 4 DPI. (f) Identification of NK1.1^{-} CD16^{-} by flow cytometry and subsequent confirmation of FcεRIγ expression. FMO = fluorescence

minus one control, DP = NK1.1^{+} CD16^{+} subset, DN = NK1.1^{-} CD16^{-} subset. Data shown from a representative animal from a pool of four mice.

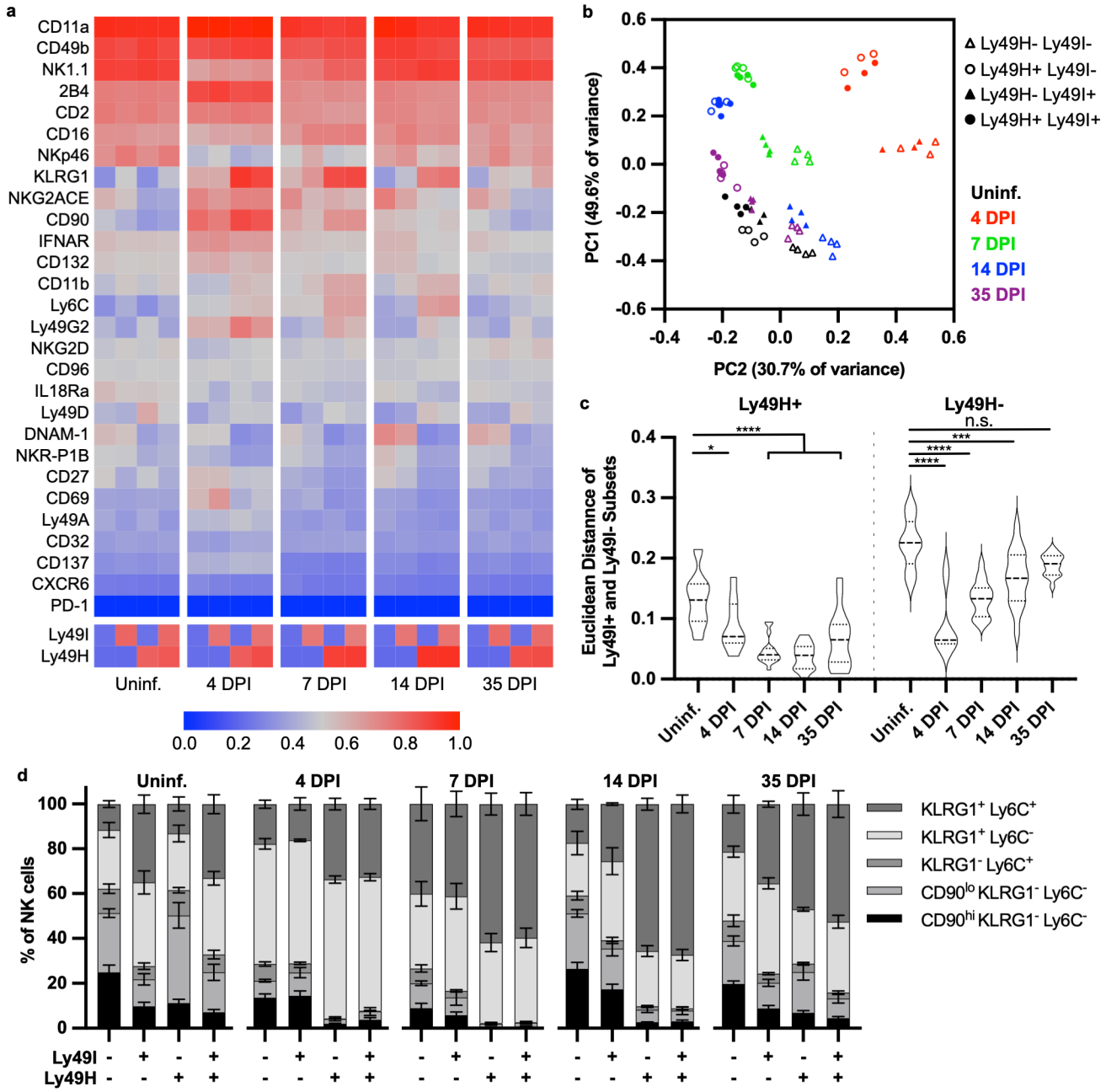

Figure 6.

Licensed and unlicensed cells increase in similarity during MCMV infection. (a) Heatmap of NK cell phenotypes for the four Ly49I/Ly49H populations at each time point. Individual events were normalized as percentage of global maximum, using the median of the top 100 events as the maximum value to account for outliers. (b) PCA of the Ly49I and Ly49H populations. (c) Euclidean similarity between the Ly49I^{+} and Ly49I^{-} populations within the Ly49H^{+} (left) and Ly49H^{-} (right) subsets. Distance measurements were made between all possible pairings for each time point. (d) Distribution of NK cell subsets within each of the four Ly49I and Ly49H compartments during MCMV infection.

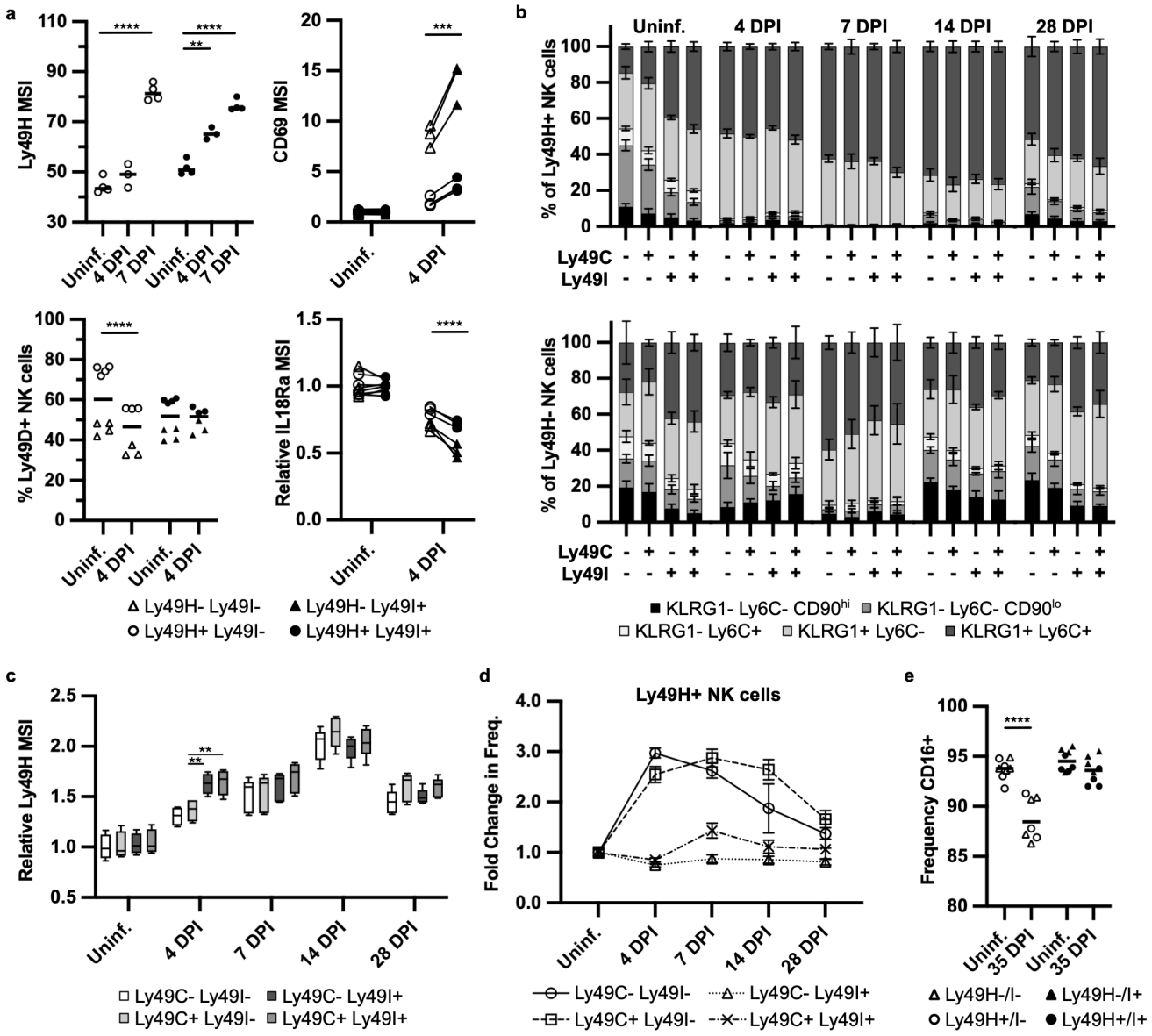

Figure 7.

The limited variability in licensed and unlicensed NK cell responses were driven by Ly49I and not Ly49C. (a) Significantly different phenotypes between licensed and unlicensed NK cells at 4 DPI as separated by the 5E6 antibody. Presented experiment is one of four repetitions. (b) Frequency of the NK cell subsets in Ly49H^{+} (top) and Ly49H^{-} (bottom) NK cells separated according to the expression or absence of Ly49C and Ly49I (n = 5 mice). (c) Change to Ly49H MSI on NK cells expressing one, both, or neither of the B6 licensing receptors during MCMV infection. (d) Magnitude of Ly49H^{+} NK cell expansion when co-expressing one, both, or neither of Ly49C and Ly49I. Measured as frequency of the total NK cell population at the indicated time point/frequency of total NK cell population in naïve uninfected mice. (e) Significantly different phenotypes between Ly49I^{+} and Ly49I^{-} NK cells at 35 DPI. * p <0.05, ** p <0.01, *** p <0.001, **** p <0.0001

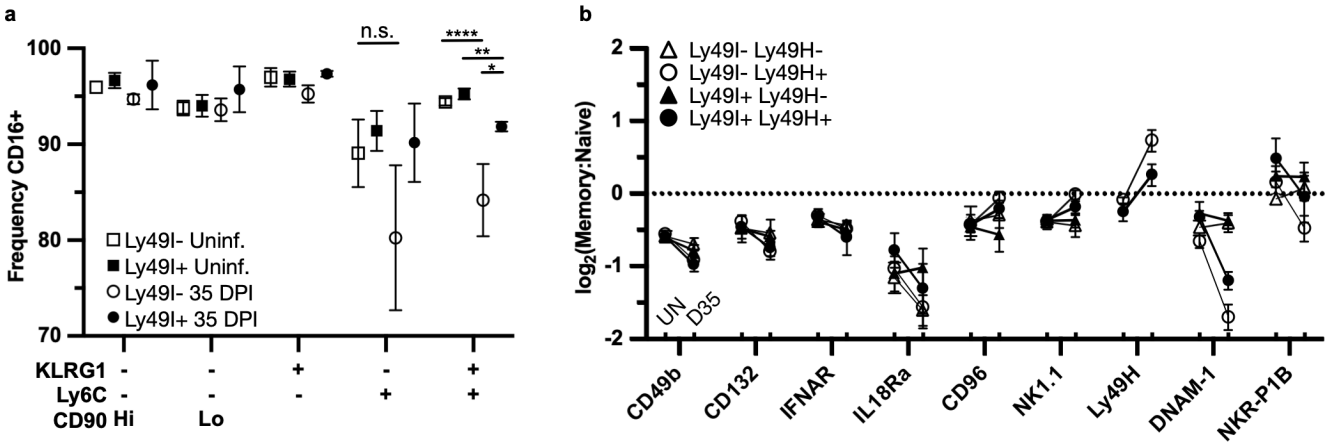

Figure 8.

Differences in memory and memory-like populations post-infection. (a) Frequency of $CD16^{+}$ expression among licensed and unlicensed NK cell subsets in uninfected and 35 DPI mice. (b) Log_2-fold difference between memory/memory-like ($KLRG1^{+}$ $Ly6C^{+}$) NK cells and immature ($CD90^{hi}$ $KLRG1^{-}$ $Ly6C^{-}$) NK cells for each of the four Ly49I and Ly49H subsets. Paired data points link corresponding populations in uninfected and 35 DPI mice. The dotted line at zero on the y-axis denotes no difference in expression between $KLRG1^{+}$ $Ly6C^{+}$ and $CD90^{hi}$ $KLRG1^{-}$ $Ly6C^{-}$ populations. Data shown is the average of four mice at each timepoint. * p <0.05, ** p <0.01 **** p<0.0001, n.s. = non-significant

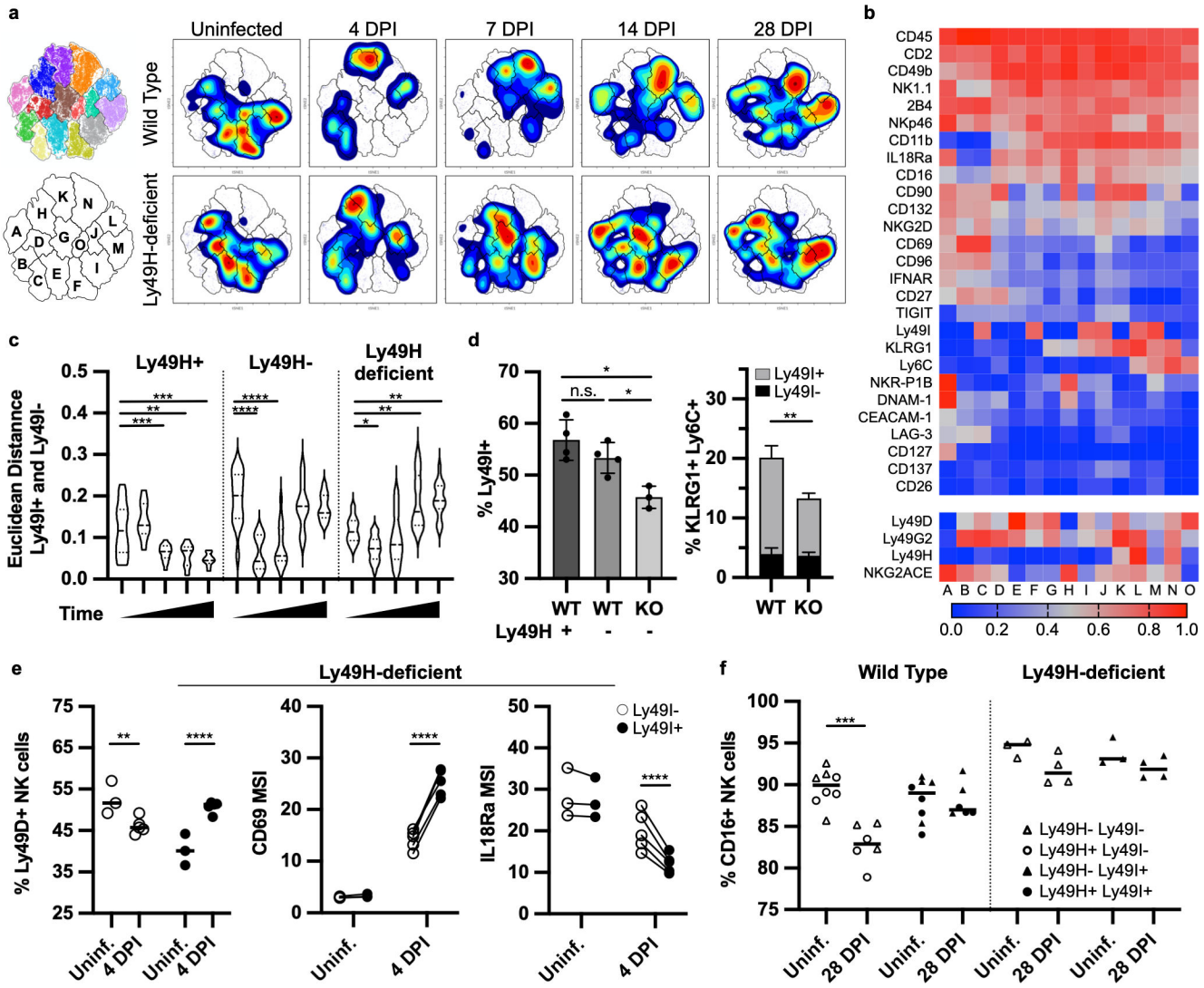

Figure 9.

Licensed and unlicensed responses resemble one another in the absence of a MCMV-specific NK cell response. (a) Clustering analysis of wild-type and Ly49H-deficient group 1 ILCs. Top left shows the overlay of cells from all time points and is colored according to metacluster; the bottom left is a guide for identification of each metacluster. The remaining plots are density plots corresponding to the indicated genotype and time point. (b) Heatmap depicting the phenotype of each metaclusters. Values represent the weighted average of constituent cluster medians normalized as percent of global maximum. (c) Euclidean similarity between the Ly49I^{+} and Ly49I^{-} populations of Ly49H^{+} NK cells (left), Ly49H^{-} NK cells from wild-type mice (middle), and NK cells from Ly49H-deficient mice (right). Distance measurements were made between all possible pairings for each time point. (d) Frequency of Ly49I^{+} cells among the Ly49H^{+}, Ly49H^{-}, and Ly49H-deficient NK cells (left) and the breakdown of Ly49I expression in the memory-like KLRG1^{+} Ly6C^{+} NK cells as a fraction of the total NK cell compartment in wild-type and Ly49H-deficient mice. (e) Phenotypic differences between licensed and unlicensed cells at 4 DPI in Ly49H-deficient

mice. (f) Frequency of $CD16^+$ NK cells in the total licensed and unlicensed NK cell populations pre- and post-infection. All timepoints represent data from four mice for each genotype, except for the uninfected Ly49H-deficient samples which had three total mice. Data shown from a single CyTOF run but is consistent with data acquired in a second experiment. * $p < 0.05$, ** $p < 0.01$ *** $p < 0.001$ **** $p < 0.0001$